SIAM J. Appl. Math.
Vol. 61, No. 3, pp. 1013–1041

SPATIAL NOISE STABILIZES PERIODIC WAVE PATTERNS IN OSCILLATORY SYSTEMS ON FINITE DOMAINS*

ALISON L. KAY† AND JONATHAN A. SHERRATT‡

Abstract. Invasions in oscillatory systems generate in their wake spatiotemporal oscillations, consisting of either periodic wavetrains or irregular oscillations that appear to be spatiotemporal chaos. We have shown previously that when a finite domain, with zero-flux boundary conditions, has been fully invaded, the spatiotemporal oscillations persist in the irregular case, but die out in a systematic way for periodic traveling waves. In this paper, we consider the effect of environmental inhomogeneities on this persistence. We use numerical simulations of several predator-prey systems to study the effect of random spatial variation of the kinetic parameters on the die-out of regular oscillations and the long-time persistence of irregular oscillations. We find no effect on the latter, but remarkably, a moderate spatial variation in parameters leads to the persistence of regular oscillations, via the formation of target patterns. In order to study this target pattern production analytically, we turn to λ–ω systems. Numerical simulations confirm analagous behavior in this generic oscillatory system. We then repeat this numerical study using piecewise linear spatial variation of parameters, rather than random variation, which also gives formation of target patterns under certain circumstances, which we discuss. We study this in detail by deriving an analytical approximation to the targets formed when the parameter λ_0 varies in a simple, piecewise linear manner across the domain, using perturbation theory. We end by discussing the applications of our results in ecology and chemistry.

Key words. oscillatory systems, periodic waves, spatial noise

AMS subject classifications. 92C50, 92C15, 35M10, 34C05

PII. S0036139999360696

1. Introduction.

Invasions are a widespread phenomenon in biology and chemistry, for instance, the spread of one animal population into a region occupied by another, the invasion of a wound space by a surrounding cell population, the movement of a reaction front as one chemical is converted to another, etc. Mathematical modeling of invasions is extensive, dating back to Fisher's work [10] on the spread of an advantageous gene and Skellam's [32] use of a reaction diffusion equation to study ecological invasion. Recent modeling work predicts that many of the most interesting invasion effects occur in oscillatory systems, such as cyclic predator-prey interactions or oscillatory chemical reactions.

Although some work has been done on spatially and/or temporally discrete models for oscillatory systems [17, 37, 29], the most widely used model type is an oscillatory system of reaction-diffusion equations. By this, we mean that the kinetic ordinary differential equations contain a stable limit cycle. In models of this type, invasions leave behind them spatiotemporal oscillations. These can be simply a periodic wavetrain moving in parallel with the invasion [6], but in many cases have the form of either a wave-train moving more rapidly than the invasion, or a complex pattern of irregular spatiotemporal oscillations [28]. These latter behaviors occur via a complex

*Received by the editors August 24, 1999; accepted for publication (in revised form) May 14, 2000; published electronically October 11, 2000.
http://www.siam.org/journals/siap/61-3/36069.html

†Mathematics Institute, University of Warwick, Coventry CV4 7AL, UK. Current address: Centre for Ecology and Hydrology, Wallingford, Oxon, OX10 8BB, UK (alkay@ceh.ac.uk). The research of this author was supported in part by a graduate studentship from the Engineering and Physical Sciences Research Council.

‡Department of Mathematics, Heriot-Watt University, Edinburgh EH14 4AS, UK (jas@ma.hw.ac.uk).

wave-train selection mechanism [28, 30], with irregular oscillations arising when the selected wave-train is unstable. Related instances of irregular oscillations generated in oscillatory reaction diffusion systems are given in [25, 9, 20].

Recently, we studied the long-term behavior of these spatiotemporal oscillations after the whole of a finite domain had been invaded, for the most important case of zero-flux conditions at the ends of the domain [13]. We considered the case when the invasion (for example, of a prey population by predators) is initiated at one end of the domain and spreads across to the other end. Numerical simulations showed that when irregular oscillations are generated behind the invasion, these persist after the whole domain has been invaded—even in very long time simulations. Contrastingly, when regular spatiotemporal oscillations were generated these died out towards the purely temporal oscillations of the limit cycle. This die-out begins with a decrease in the spatial frequency of the oscillations at one side of the domain, which then progresses across the domain, with a simultaneous progression of increase in the amplitude of the oscillations (to the limit cycle amplitude). In order to study the manner of the die-out in more detail we used a caricature model, which showed the same phenomena of persistence of irregular oscillations and die-out of regular oscillations in numerical simulations. Analysis of this simpler system then gave an approximation to the transition fronts occuring during the die-out, and a measure of the rate of die-out, in terms of model parameters, which can be related back to the parameters in more general oscillatory systems in some cases.

The results of this previous work can only be applied to real oscillatory systems once two key questions have been answered. First, are the phenomena seen in homogeneous environments robust to the introduction of inhomogeneities? In addition, will inhomogeneities result in new phenomena, not seen in the homogeneous case? Examples of the latter have been observed in nature. In the Belousov–Zhabotinskii reaction it is known that target patterns almost always have an impurity in the center, and so occur in fewer numbers in a highly purified system [38]. It is also thought that inhomogeneities are necessary for the formation of spiral waves in cardiac tissue [27]; it is these spiral waves which result in abnormal heart rhythms.

There are clearly many ways in which spatial inhomogeneity can be created. We focus on achieving this inhomogeneity by spatial variation of parameters, and there are two very different means of accomplishing this; either there is a simple, functional variation with spatial position imposed on some parameter(s), or the variation is "noisy"—randomly generated. Much of the work on the latter has been with spatiotemporal noise, rather than the purely spatial noise which we consider. An exception is the work, on discrete time and space models of host-parasitoid interactions, by Comins, Hassell, and May [5] and Holt and Hassell [12], in which it is shown that noisy spatial variation of demographic parameters can stabilize the system. In particular, in [5], it is demonstrated that spiral patterns and spatiotemporal chaos remain clearly evident even with quite high levels of noisy patch-to-patch variation. Lattice patterns, however, are easily disrupted.

The possibilities for functional variation of parameters are huge, and so the consequences cannot be described generally, but we discuss various examples below. For reaction-diffusion equations, explicit spatial variation has been shown to have important consequences in the areas of traveling wave propagation and pattern formation. In [39], Xin considered a scalar reaction-diffusion equation with a cubic kinetic term, where the diffusion coefficient is allowed to vary with spatial position. He showed that, if the variation of the diffusion coefficient from its mean is sufficiently large, then traveling waves no longer exist, so that a wave front will begin to propagate from given initial conditions, but will then stop advancing—a phenomenon known as quenching. A similar result was found in [33], where Sneyd and Sherratt model calcium wave propagation in inhomogeneous media. Calcium waves can be either excitable or self-oscillatory. In the excitable regime, the authors used a scalar reaction-diffusion equation on a domain with a "gap"—a region where the kinetics are set to zero—to derive a critical gap width, above which waves cannot propagate. In the oscillatory regime, they used a piecewise constant spatial variation of the kinetics, in a system of two reaction-diffusion equations, with periodic regions where the kinetics are set to zero, and demonstrated numerically how these passive regions disturb the periodic plane waves which propagate behind an invading front. Piecewise constant spatial variation was also used by Shigesada [31] to study the effects of a heterogeneous environment on the spread of a single species. There, an invasion condition was determined, which depended on the patch sizes and on the diffusivities and growth rates of the species within the two different types of patch.

The consequences of spatial variation for pattern formation are less obvious, but just as important in reality. Although the Turing mechanism for pattern formation has been widely studied, the usual assumption of a uniform domain often does not fit with that used in experiments or in natural pattern forming systems. It has been shown that allowing spatial variation of parameters, in ways which are more applicable to experiments or nature, can lead to quite major alterations in the patterns which can be expected at different points in parameter space, and the bifurcation sequences observed [1, 2].

Spatial heterogeneity has also been shown to have quite major effects on interacting populations. Using a system of two weakly coupled reaction-diffusion equations with spatial variation of the kinetics, Cantrell, Cosner, and Hutson [3] showed that the spatial heterogeneity resulted in the permanence of populations which would otherwise have become extinct. Also, Pascual [24] showed that large-scale spatial variation in kinetics can induce chaotic oscillations in cyclic predator-prey systems. Spatial heterogeneity can also lead to a different outcome of competition than that which occurs in a spatially homogeneous environment [23, 4], and to altered success of the predator in predator-prey systems, depending upon the location of favorable hunting grounds [4].

The effects of spatial variation have also been investigated in spatially discrete systems. Chains of coupled oscillators can be used to model lamprey locomotion, and any variation of parameters along the length of the fish could be important to its swimming efficiency. Kopell and Ermentrout [16] analyzed a system of N weakly coupled oscillators, in the continuum limit as $N \to \infty$, where the natural frequency of the oscillator, and its coupling strength to each of its neighbors, were allowed to vary smoothly and slowly along the chain. A special case which they consider is where there is a local region of lower/higher natural frequencies (with coupling strengths equal along the chain). They show that a sufficiently large frequency difference can result in effects not localized to the region of the chain with altered frequencies—including reversal in direction of the wave from the changed region to one of the boundaries. Similar effects are shown to result from local regions of weakened coupling.

The existence of target pattern solutions of reaction-diffusion systems on infinite domains has been extensively studied. Hagan [11] showed that stable target patterns exist whether or not impurities are present, but that they will arise from typical initial conditions only if impurities which tend to locally increase the frequency are present.

Kopell [15] used a similar approach in the special case of λ–ω systems, showing that such a local increase in frequency is sufficient to produce one- or two-dimensional target patterns, but that it has to be sufficiently large, in magnitude and extent, to produce three-dimensional patterns.

In this paper, we consider the effect of spatial inhomogeneities on the persistence of oscillations on a finite (one-dimensional) domain with zero-flux boundary conditions. Although our analytical results are quite general we use cyclical predator-prey systems as a case study, in order to have a specific application in mind. We begin (section 2) by presenting the results of numerical simulations of invasion of a noisy domain for predator-prey systems in the oscillatory regimes, considering the long-term behavior, after the invasion front has crossed the domain. We use the term "noisy domain" to mean that the parameters vary randomly across the spatial domain, but are fixed in time. Then, in sections 3 and 4, we use a caricature model to study the behavior in more detail; first verifying that the same behavior is seen for noisy variation of parameters, then using a piecewise linear change in the parameters across the domain.

2. Spatially varying parameters in predator-prey systems. In this section we present numerical results on the invasion of a prey population by predators on a noisy domain. Our results have ecological significance, which will be discussed at the end of the paper; however, we discuss the predator-prey example at this stage in order to motivate, via a concrete example, the work on a more generic system in sections 3 and 4.

We consider reaction-diffusion systems with the form

$$\frac{\partial h}{\partial t} = D_h \frac{\partial^2 h}{\partial x^2} + f_h(h, p, x), \tag{1a}$$

$$\frac{\partial p}{\partial t} = D_p \frac{\partial^2 p}{\partial x^2} + f_p(h, p, x), \tag{1b}$$

where $p(x,t)$ and $h(x,t)$ denote predator and prey densities, respectively, at time t and position x in a one-dimensional spatial domain and D_p and D_h are the diffusion coefficients. Biologically realistic kinetic terms f_p and f_h will have two nontrivial equilibria, a "prey-only" steady state which we take to be $p = 0$, $h = 1$ by suitable rescaling, and a "coexistence" state, $p = p_s$, $h = h_s$. For cyclical populations, this coexistence state will also be unstable and will lie inside a stable limit cycle in the kinetic phase plane. We have considered three standard sets of predator-prey kinetics, all of which have such a stable limit cycle for appropriate parameter values:

$$f_h(h,p) = h(1-h) - p(1 - e^{-c(x)h}), \qquad f_p(h,p) = b(x)p(a(x) - 1 - a(x)e^{-c(x)h}), \tag{2}$$

$$f_h(h,p) = h(1-h) - \frac{hp}{h + c(x)}, \qquad f_p(h,p) = \frac{a(x)ph}{h + c(x)} - b(x)p, \tag{3}$$

$$f_h(h,p) = h(1-h) - \frac{a(x)hp}{h + c(x)}, \qquad f_p(h,p) = b(x)p\left(1 - \frac{p}{h}\right). \tag{4}$$

Here $a(x)$, $b(x)$, and $c(x)$ are positive parameters in all cases. Pascual [24] has previously studied models of this type with large-scale, linear variations in parameter values, showing that this can induce chaotic oscillations. Here we consider the quite different case of small spatial oscillations in parameter values.

We begin by presenting the results of numerical simulations of invasion on finite spatial domains where the kinetic parameters a, b, c are allowed to vary in a random way across the domain. We solve (1) with (2), (3) or (4) numerically on $0 < x < L$, with zero-flux boundary conditions at $x = 0$ and $x = L$, and initial conditions $h = 1,\ p = 0$ on $l < x < L$ for some $l \ll L$, with a nonzero initial value of p on $0 < x < l$. This corresponds to the introduction of predators at one edge of a domain that is otherwise occupied entirely by prey. However, we also initially generate a random variation of some or all of the kinetic parameters (a, say) across the domain. We do this by choosing "average" values for each of the parameters (a_{av}) and a maximum percentage by which we will allow them to vary (P). We then generate the values of each parameter at each point in our spatial grid by using a random number generator to choose a number between -1 and 1 (ρ, say, calculated from a uniform distribution), and setting $a = a_{av} + a_{av} \times \rho \times P/100$. Thus we do not change the sign of any of the parameters (all of which are positive), so the nature of the species interactions remains unchanged; we are simply changing the *relative* effects of each of the terms at each space point, to model varying quality of the habitat. (Note that, if the percentage variation is large enough, we may, of course, be choosing the parameters at a point in space in such a way that the stable limit cycle does not exist at that point.) We then solve using a Crank–Nicolson scheme, in order to determine the effect that the spatial noise in the parameter values has on the observed behavior of persistence of oscillations after invasion; the corresponding behavior for homogeneous domains was described in [13] and was summarized in section 1.

Numerical simulations for a range of parameters show a clear pattern of behavior. As one might expect, the noisy spatial variation of the parameters has no effect on the persistence of irregular oscillations after the invasion of a front with an irregular wake. A very small amount of noise similarly has no noticeable effect on the die-out of the regular oscillations after the invasion of a front with a regular wake (Figure 1(a)). Specifically, the die-out occurs as a transition moving across the domain in the opposite direction to the invasion, with a gradual increase in spatial wavelength and amplitude of the spatiotemporal oscillations. However, we found that a moderate level of noise could lead to persistence of regular oscillations, but usually of a different spatial frequency than that generated behind the invasion, and with sections of the domain having the wave-trains traveling in opposite directions (Figures 1(b) and 1(c)). The regular oscillations produced do, though, have a slightly noisy modulation of their regular shape. The frequency of the periodic plane-wave selected appears to depend upon the amount of noise—the larger the noise percentage the higher the frequency—until too large a noise percentage results in the breakdown of the regular-looking solution to an irregular-looking one (Figure 1(d)).

The same results were seen if we chose the parameter values randomly at fewer of the space points, interpolating for the values at intervening points, or if just a small region of the domain had parameter noise, with the parameters taking their average values outside of this region.

If we continue the integration from a time long after an invading front has crossed the domain, resetting the values of the parameters at each space point to their average values, the periodic plane-waves again die out from the whole of the domain. This occurs in a manner similar to that after the invasion of a wave front with a

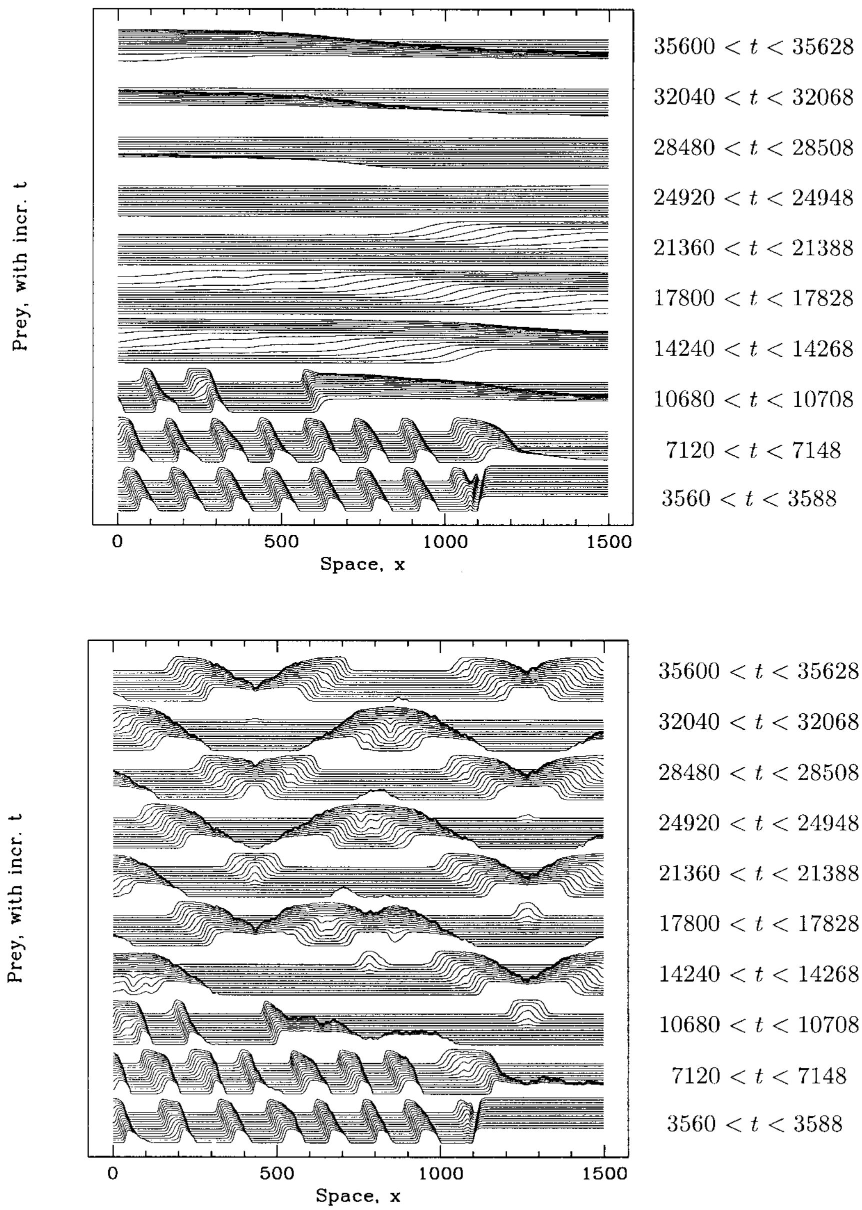

a)

b)

FIG. 1. *Numerical simulations of invasion in a cyclic predator-prey system, showing the behavior after an invasive front with a regular oscillatory wake has reached the far side of a finite domain, with zero-flux boundary conditions and spatially noisy parameters.* (a) $P = 0.25\%$, (b) $P = 10\%$, (c) $P = 20\%$, (d) $P = 90\%$. *Graphs* (b) *and* (c) *clearly illustrate the persistence of the regular oscillations, the latter with just one point on the domain from which periodic plane-waves appear to be diverging, the former with two; in complete contrast to the case with a homogeneous domain* [13] *and graph* (a), *with a very small noise percentage. Graph* (d) *illustrates the apparently irregular solution obtained from the regular wake with a high noise percentage on the domain. The solutions shown are for* (1) *with kinetics* (3) *with noise on the parameters a and b but not c, for parameter values* $D_h = D_p = 1$, $a_{av} = 0.15$, $b_{av} = 0.05$, *and* $c_{av} = 0.2$.

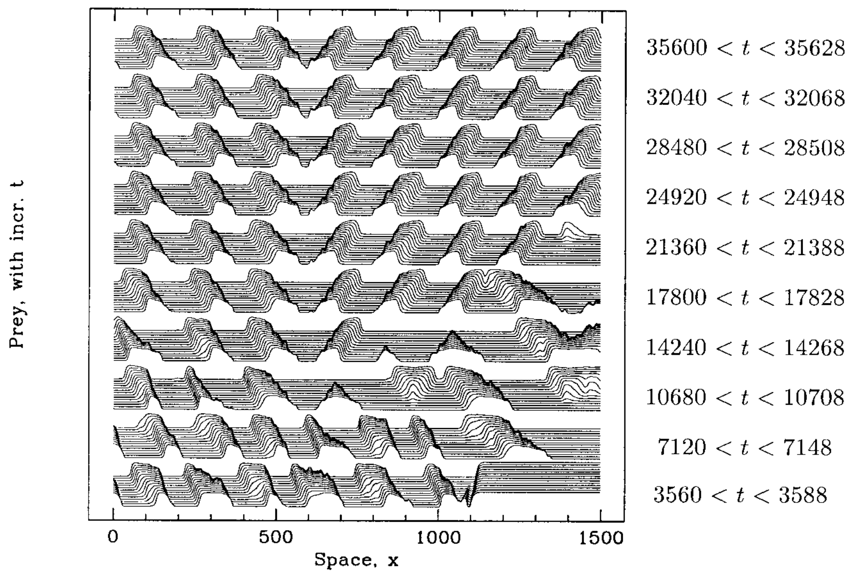

c)

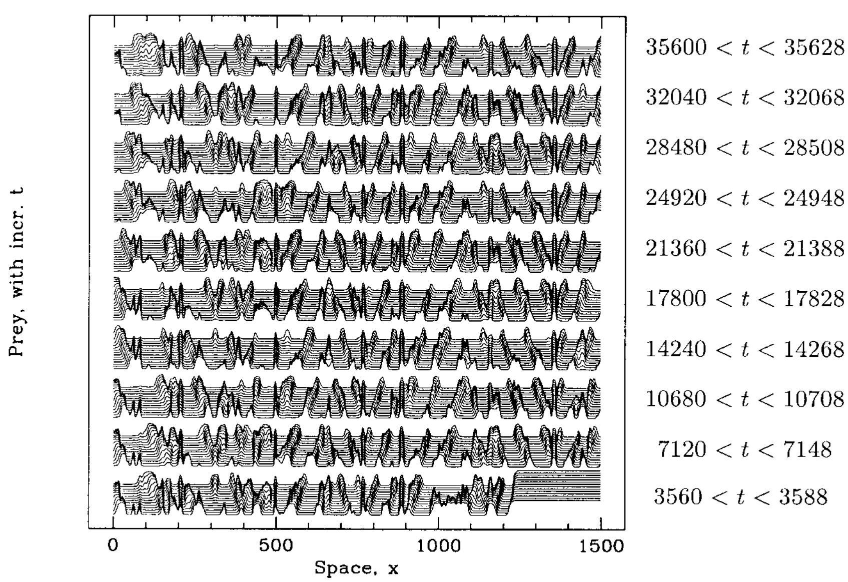

d)

FIG. 1. *continued.*

regular wake into an homogeneous domain, but with the decrease in frequency of the spatial oscillations occurring first at the points from which the wave-trains appear to be diverging, and progressing outwards from there, rather than beginning at one of the boundaries. The solution then evolves towards purely temporal oscillations, corresponding to the limit cycle of the kinetics. This die-out to the purely temporal oscillations of the limit cycle still occurs in most cases for the irregular-looking behavior produced from regular wakes on domains with large noise percentages. We have, though, found cases where irregular oscillations are produced from regular wakes by the high noise percentages and persist even when the noise is stopped.

We note here that we can expect there to be some dependence of results on the size of the domain used. In cases where dynamic spatial patterning can appear, it will have some characteristic length scale associated with it, and in order for the pattern to be apparent we require the domain to be sufficiently larger than this pattern's length scale; just as the form of Turing patterns is dependent on the size of the domain [21, pp. 436–448]. We have always worked with domains which are large compared to the period of the wave-train generated behind invasion.

The ecological implications of these results will be discussed in section 5. Prior to this, we study in more detail the way in which spatial heterogeneity can lead to persistence of regular oscillations, using a caricature system of oscillatory reaction-diffusion equations.

3. Spatially varying parameters in λ–ω systems.

Background. We have been unable to make any progress studying the predator-prey models (1) with (2), (3) or (4) analytically, for general parameter values. However, there is a special case in which the systems are much more amenable to analysis, namely for kinetic parameters close to the Hopf bifurcation, and for equal predator and prey diffusion coefficients. In this case the kinetics can be approximated by the Hopf normal form, giving

$$\frac{\partial u}{\partial t} = \frac{\partial^2 u}{\partial x^2} + \lambda(r)u - \omega(r)v, \tag{5a}$$

$$\frac{\partial v}{\partial t} = \frac{\partial^2 v}{\partial x^2} + \omega(r)u + \lambda(r)v, \tag{5b}$$

where u and v represent appropriate linear combinations of the predator and prey densities p and h. Here $r = (u^2 + v^2)^{\frac{1}{2}}$, with $\lambda(r) = \lambda_0(x) - \lambda_1 r^2$ and $\omega(r) = \omega_0(x) - \omega_1 r^2$, where $\lambda_0, \lambda_1 > 0$, and we allow λ_0, ω_0 to vary with spatial position x. Note that the system (5) is very general, being the normal form of any oscillatory reaction-diffusion system close to Hopf bifurcation, provided the variables have the same diffusion coefficient. Thus our calculations will apply to a range of applications in addition to ecology, and this is discussed further in section 5.

Reaction-diffusion systems of the form (5) are known as "λ–ω systems," and were first studied by Kopell and Howard [14]. The key to the analytical study of such systems is to work in terms of polar coordinates in the u-v plane, r and $\theta = \tan^{-1} v/u$, in terms of which (5) becomes

$$\frac{\partial r}{\partial t} = \frac{\partial^2 r}{\partial x^2} - r\left(\frac{\partial \theta}{\partial x}\right)^2 + r(\lambda_0(x) - \lambda_1 r^2), \tag{6a}$$

$$\frac{\partial \theta}{\partial t} = \frac{\partial^2 \theta}{\partial x^2} + \frac{2}{r}\frac{\partial r}{\partial x}\frac{\partial \theta}{\partial x} + (\omega_0(x) - \omega_1 r^2). \tag{6b}$$

From this formulation, when $\lambda_0(x) \equiv \lambda_0$ and $\omega_0(x) \equiv \omega_0$, it is clear that there is a spatially homogeneous circular limit cycle solution, with amplitude (radius) $r_c = (\lambda_0/\lambda_1)^{\frac{1}{2}}$. Moreover, there is a family of periodic wave-train solutions, which are also circular in the u-v plane, with amplitude $\hat{r}$ for any $\hat{r} < r_c$. The form of these wave-train solutions is easily determined: substituting $r(x,t) = \hat{r}$, a constant, into (6) implies $\theta(x,t) = \sqrt{\lambda(\hat{r})}x + \omega(\hat{r})t + \theta_0$, where θ_0 is an arbitrary constant, which may be set to zero without loss of generality. Thus the periodic waves have the form

$$\begin{aligned} u(x,t) &= \hat{r}\cos\theta(x,t) = \hat{r}\cos(\sqrt{\lambda(\hat{r})}x + \omega(\hat{r})t), \\ v(x,t) &= \hat{r}\sin\theta(x,t) = \hat{r}\sin(\sqrt{\lambda(\hat{r})}x + \omega(\hat{r})t). \end{aligned}$$

Thus we have a sinusoidal periodic plane wave moving with speed $\omega(\hat{r})/\sqrt{\lambda(\hat{r})}$ in the negative x-direction. There is also the mirror image wave, where $\theta(x,t) = -\sqrt{\lambda(\hat{r})}x + \omega(\hat{r})t$, which moves with the same speed in the positive x-direction.

Kopell and Howard [14] derived a stability condition for the periodic wave-train solutions of λ–ω systems, which in the case of (6) with $\lambda_0(x) \equiv \lambda_0$ and $\omega_0(x) \equiv \omega_0$ shows that the periodic plane waves are stable if and only if their amplitude $\hat{r} > \hat{r}_c$, where $\hat{r}_c = \left[\frac{2\lambda_0}{\lambda 1}\left(\frac{\lambda_1^2+\omega_1^2}{3\lambda_1^2+2\omega_1^2}\right)\right]^{1/2}$. The existence of this precise stability result is in sharp contrast to more general oscillatory reaction-diffusion systems, for which results on stability of periodic waves are quite limited [22, 19].

Numerical simulations with parameter noise. We cannot use λ–ω systems to mimic the invasion process used for predator-prey equations, as there is no equivalent of the prey-only equilibrium, but we can investigate persistence of oscillations by using appropriate initial conditions. Thus to investigate the persistence of regular oscillations on finite domains with zero-flux boundary conditions we solve the equations numerically with initial conditions consisting of a periodic plane-wave of stable amplitude $\hat{r} > \hat{r}_c$ on the whole of the domain (which is taken sufficiently large compared to the period of the plane-wave). We consider behavior arising from these initial conditions when the parameters λ_0 and ω_0 vary randomly with spatial position x, in the same way as was described for the parameters in the predator-prey equations in the preceding section.

Our results showed that, for a very small variation of the parameters, the regular oscillations still die out, towards the purely temporal oscillations of the limit cycle (although this is now "noisy"—its amplitude varies slightly with x) (Figure 2(a)). Figure 3 illustrates this die-out plotted in terms of r and θ_x, and clearly shows that it is occuring via transition fronts in r and θ_x, starting from the right-hand side and progressing across the domain from there. This is identical to the die-out of regular oscillations seen on homogeneous domains, and thus the analysis done in that case [13], where approximations to the transition fronts were derived and an estimate of the rate of die-out in terms of parameters was obtained, still applies for sufficiently small noisy variations.

For larger parameter variations though, numerical simulations again show persistence of regular oscillations. However, these oscillations do not consist just of a single wave-train traveling across the domain; rather the domain is divided into at least two regions, with a wave-train traveling in the opposite direction, but in phase, in neighboring regions. That is, we get one-dimensional versions of a series of either target patterns or shocks (Figure 2(b)). Note that the term "target pattern" refers to wave-trains *diverging* from a point, meaning that the group velocities are directed

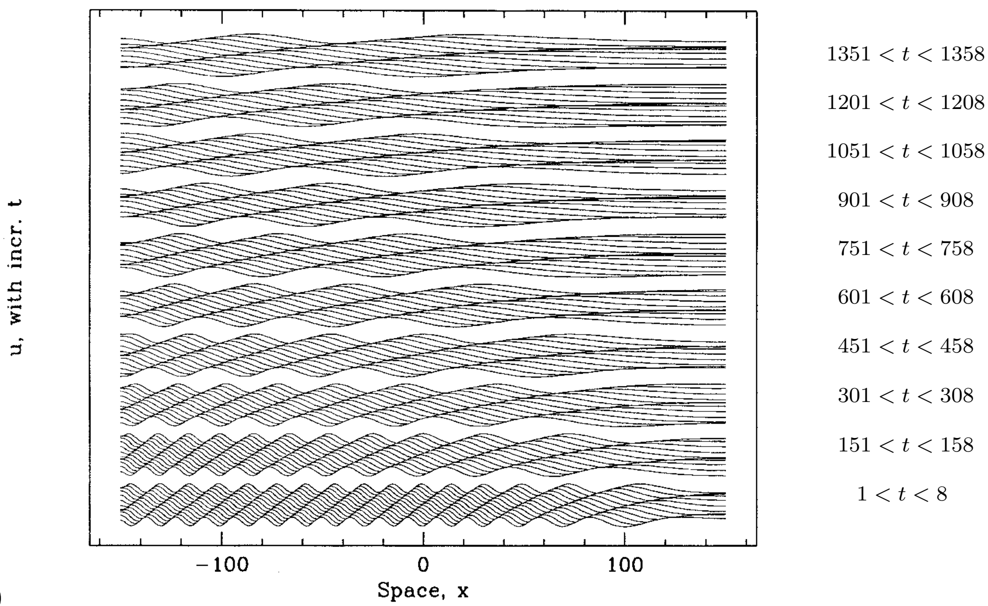

a)

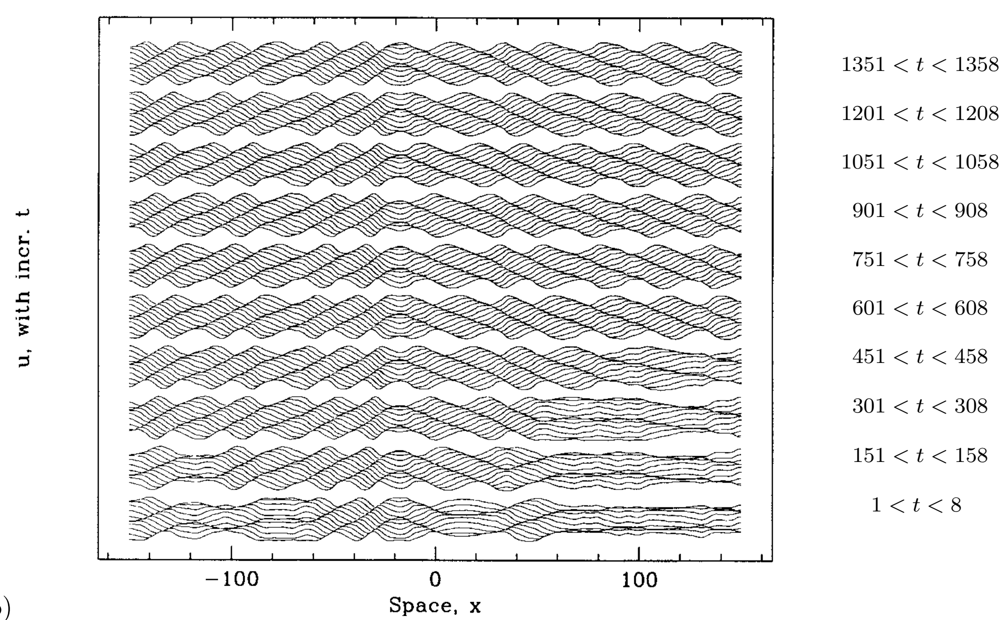

b)

Fig. 2. *Numerical simulations showing* (a) *the die-out towards the limit cycle and* (b) *the formation of a target pattern, on a noisy domain. The solutions are for* (5), *with, respectively, a* 0.25% *and* 15% *variation in* λ_0, ω_0 *(around their average values of* 1 *and* $-1/2$*, respectively) and with* $\lambda_1 = \omega_1 = 1$*, from an initial periodic plane-wave of stable amplitude* $\hat{r} = 0.9$.

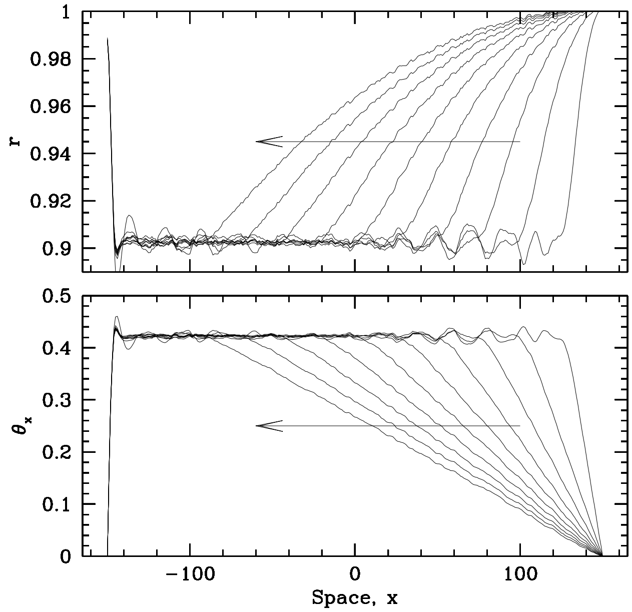

FIG. 3. *An illustration of the solution shown in Figure* 2, *replotted in terms of* r *and* θ_x. *This shows that the initial regular oscillations are dying out in a way which is identical to that which occurs on a homogeneous domain, except with a noisy modulation. As in Figure* 2, λ_0 *and* ω_0 *have a maximum noisy variation of* 0.25% *around average values of* 1 *and* -0.5, *respectively, and* $\lambda_1 = \omega_1 = 1$. *The solutions are plotted as a function of space* x *(*$-150 < x < 150$*), at equally spaced times* (*interval* 20); *the arrows indicate the direction in which the solutions evolve as time increases.*

outwards—the phase velocities could be going in either direction, depending on the exact form of $\omega(\cdot)$; the case with wave-trains *converging* on a point (group velocities directed inwards) is usually referred to as a "shock."

The changing of direction of the wave-trains can be seen more clearly by replotting in r, θ_x coordinates, where sections of "constant" r and θ_x show the periodic plane-waves (although there will be a noisy modulation of these constant values), and a change in sign of θ_x shows the change in direction of the wave-train (Figure 4). The way in which θ_x changes sign—that is, whether it changes from negative to positive or from positive to negative as x increases—(along with the sign of $w(\cdot)$ evaluated at the wave-train amplitude) then tells us whether we actually have a target or a shock. This formulation of the results also allows us to see that a steady state has been reached, as continuing the integration further results in no significant change to the $r,\ \theta_x$ plots. However, if we continue the integration having reset the parameters to their average values, we see the periodic plane-waves dying out in a manner similar to that seen on the homogeneous domain, except that it occurs symmetrically from either side of the point at which the target pattern was centered, rather than progressing inwards from one side of the domain.

Again, to confirm that we are not seeing a numerical artifact, we allow noisy variation of the parameters at fewer space points, interpolating for the values at intervening points, or having just one section of the domain with noisy parameters, with the parameters taking their average values on the rest of the domain. These simulations still result in target pattern solutions appearing. The solutions in each

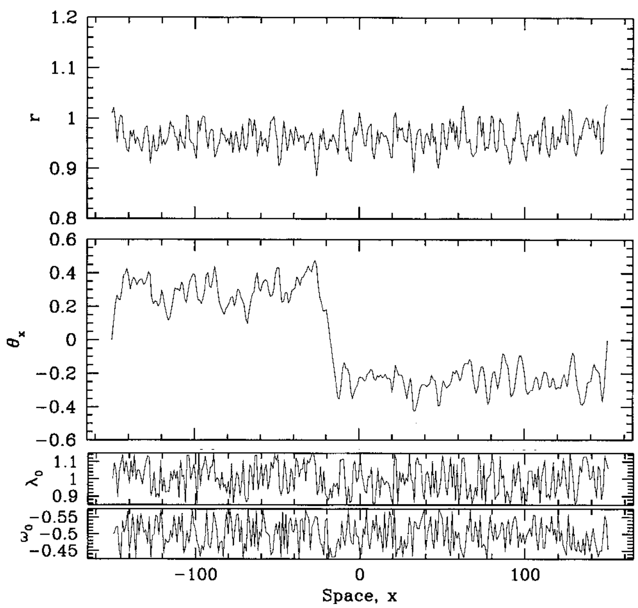

FIG. 4. *An illustration of the final time-plot of the solution in Figure* 2(b), *replotted in terms of* r *and* θ_x. *This shows clearly the sections of "constant"* r *and* θ_x *values to either side of a change in sign of* θ_x, *so illustrates that we have plane-waves converging on/diverging from a central point; a shock/target. It is actually a target rather than a shock, as the group speed of the plane-wave to the left of the point is negative and that to the right is positive, so the two waves are diverging from the point. Due to our choice of the function* $\omega(r) = -1/2 - r^2$, *the phase velocities are directed towards the point, and so the waves will appear (on a graph where the time interval between successive time plots is sufficiently small) to be converging on the point.*

case are essentially the same; the only difference being a slightly longer transitionary period.

Numerical simulations with piecewise linear $\boldsymbol{\lambda_0}$ and $\boldsymbol{\omega_0}$. It is obviously difficult to get analytic results, even in λ–ω systems, when we have allowed noisy variation of the parameters. In this section then, we consider an explicit functional variation of the parameters, which we will show gives similar numerical results to those for noisy parameters—in particular, giving one-dimensional target patterns if the domain is sufficiently large—and then, in section 4, we attempt to obtain an approximate solution in this case. Work in this simpler case may also give us some insight into why target patterns are produced when the parameters are allowed to vary randomly across the domain.

Before we begin, we use rescalings to simplify the system. The most general system in our required form is

$$\frac{\partial \widetilde{r}}{\partial \widetilde{t}} = \frac{\partial^2 \widetilde{r}}{\partial \widetilde{x}^2} - \widetilde{r}\left(\frac{\partial \widetilde{\theta}}{\partial \widetilde{x}}\right)^2 + \widetilde{r}(\widetilde{\lambda_0}(\widetilde{x}) - \lambda_1 \widetilde{r}^2), \tag{7a}$$

$$\frac{\partial\widetilde{\theta}}{\partial\widetilde{t}} = \frac{\partial^2\widetilde{\theta}}{\partial\widetilde{x}^2} + \frac{2}{\widetilde{r}}\frac{\partial\widetilde{r}}{\partial\widetilde{x}}\frac{\partial\widetilde{\theta}}{\partial\widetilde{x}} + (\widetilde{\omega_0}(\widetilde{x}) - \omega_1\widetilde{r}^2)\,; \tag{7b}$$

we will drop the tildes after rescaling the variables. Here the variation of $\widetilde{\lambda_0}$, $\widetilde{\omega_0}$ with $\widetilde{x}$ which we consider is piecewise linear, taking a constant value in most of the domain, and a different constant value in a region in the center, with a linear variation between the two values. Mathematically, we set $\widetilde{\lambda_0}(\widetilde{x}) = \overline{\lambda_0}(1 + \rho_\lambda\varepsilon\widetilde{f}(\widetilde{x}))$ and $\widetilde{\omega_0}(\widetilde{x}) = \overline{\omega_0}(1 + \rho_\omega\varepsilon\widetilde{f}(\widetilde{x}))$, where $\overline{\lambda_0}$, $\overline{\omega_0}$ are constants ($\overline{\lambda_0} > 0$), $\rho_{\lambda,\omega}$ are -1, 0 or $+1$, ε is a small parameter, the domain is $-\widetilde{x}_{\max} < \widetilde{x} < \widetilde{x}_{\max}$ and $\widetilde{f}(\cdot)$ reflects the piecewise linear variation and is defined explicitly below. We simplify the system using the rescalings

$$\begin{aligned} &\Omega_0 = \overline{\omega_0}/\overline{\lambda_0}, && \widetilde{x} = x/\sqrt{\overline{\lambda_0}}, && \widetilde{\theta} = \theta, \\ &\Omega_1 = \omega_1/\lambda_1, && \widetilde{t} = t/\overline{\lambda_0}, && \widetilde{r} = r\sqrt{\overline{\lambda_0}/\lambda_1}, \end{aligned} \tag{8}$$

in terms of which equation (7) becomes

$$\frac{\partial r}{\partial t} = \frac{\partial^2 r}{\partial x^2} - r\left(\frac{\partial\theta}{\partial x}\right)^2 + r(\lambda_0(x) - r^2), \tag{9a}$$

$$\frac{\partial\theta}{\partial t} = \frac{\partial^2\theta}{\partial x^2} + \frac{2}{r}\frac{\partial r}{\partial x}\frac{\partial\theta}{\partial x} + (\Omega_0\omega_0(x) - \Omega_1 r^2), \tag{9b}$$

where $\lambda_0(x) = 1+\rho_\lambda\varepsilon f(x)$, $\omega_0(x) = 1+\rho_\omega\varepsilon f(x)$, and $f(x) = \widetilde{f}(x/\sqrt{\overline{\lambda_0}})$. Thus we have a system where the limit cycle on a homogeneous domain ($f \equiv 0$) has amplitude 1. To be specific, we take $\Omega_0 < 0$, $\Omega_1 > 0$, which implies that $\omega(r) = \Omega_0\omega_0(x) - \Omega_1 r^2 < 0$ for all $0 < r < 1$. (This makes it easier to distinguish targets from shocks). We take $f(\cdot)$ to have the form

$$f(x) = \begin{cases} \dfrac{x_2 + x}{x_2 - x_1} & \text{on } -x_2 < x < -x_1, \\ 1 & \text{on } -x_1 < x < \ x_1, \\ \dfrac{x_2 - x}{x_2 - x_1} & \text{on } \quad x_1 < x < \ x_2, \\ 0 & \text{otherwise,} \end{cases} \tag{10}$$

where x_1, x_2 satisfy $0 < x_1 < x_2 < x_{\max}$.

In our numerical simulations of (9), we expect the size of the domain to affect the results, and so we consider the specific cases $x_{\max} = 10$ and $x_{\max} = 100$, with $x_1 = x_2/2 = x_{\max}/4$. For a fixed value of ε (taken to be 0.01), we can summarize our results as follows.

When we decrease λ_0 or increase ω_0 in a region in the center of the domain:

- For $x_{\max} = 100$, we observe bands of periodic plane waves to either side of the central region, converging (with *phase* velocity) to the center. Thus a change in sign of θ_x occurs at $x = 0$, changing from positive to negative as x increases through zero. That is, we obtain a target pattern solution (Figure 5(a)).
- For $x_{\max} = 10$, there is still a change in sign of θ_x at $x = 0$, however there are no obvious periodic plane-waves (Figure 5(b)).

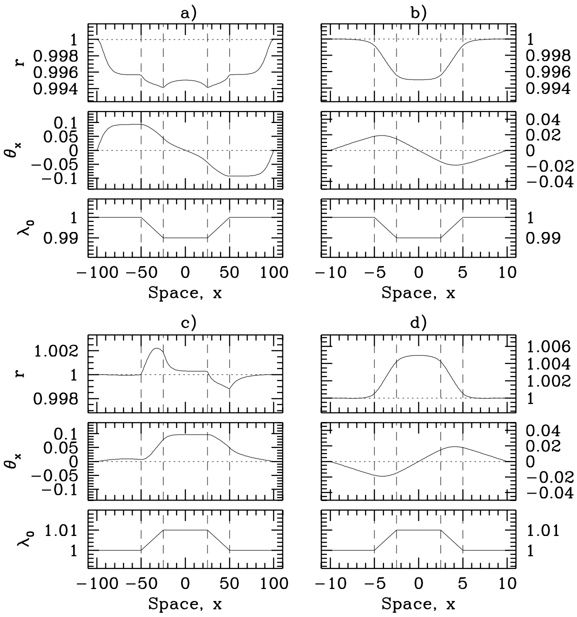

FIG. 5. *Graphs illustrating examples of r and θ_x plots in each of four cases:* (a) $x_{\max} = 100$, λ_0 *decreased* ($\rho_\lambda = -1$), (b) $x_{\max} = 10$, λ_0 *decreased* ($\rho_\lambda = -1$), (c) $x_{\max} = 100$, λ_0 *increased* ($\rho_\lambda = +1$), (d) $x_{\max} = 10$, λ_0 *increased* ($\rho_\lambda = +1$), *showing the qualitative differences obtained (solid lines). The dashed lines indicate the region boundaries* $(-x_2, -x_1, x_1, x_2)$. *All of the plots are solutions of* (9) *with* $\rho_\omega = 0$ ($\omega_0(x) \equiv 1$), $\Omega_0 = -1/2$, $\Omega_1 = 1$, *where* $f(x)$ *is given in* (10) *and* $\varepsilon = 0.01$, *plotted at* $t = 2000$, *from initial conditions of a periodic plane-wave of stable amplitude* $\hat{r} = 0.9$.

When we increase λ_0 or decrease ω_0 in the center of the domain:

- For $x_{\max} = 100$, we observe a small band of periodic plane-waves in the central region, with little/no spatial variation outside of the region. The plane-waves move in one direction; no change in sign of θ_x occurs (Figure 5(c)).
- For $x_{\max} = 10$, we now get a change in sign of θ_x at $x = 0$, but changing from negative to positive as x increases through zero. No periodic plane waves are evident (Figure 5(d)).

If both λ_0 and ω_0 are changed, by the same amount ε,

- our results suggest that the form of the solution is determined by the direction of change of λ_0. For example, when both λ_0 and ω_0 are increased on a domain with $x_{\max} = 100$, we see just one band of periodic plane waves, in the center of the domain—*not* a target pattern, as would occur if ω_0 was increased but λ_0 remained unchanged across the domain.

Discussion of results of numerical simulations. On a small domain, we expect that we may not see spatial variation, as it will be the change in the parameter values in the center of the domain which will select the wavelength of the periodic plane-waves, and if this wavelength is larger than the domain size, the periodic plane-waves will not be seen. This domain size effect is demonstrated numerically by doing simulations on the small domain with larger values of ε; eventually ε is large enough for small regions with constant r and θ_x to begin to develop—corresponding to periodic plane-waves beginning to form. (We remark, however, that when ε is taken too large,

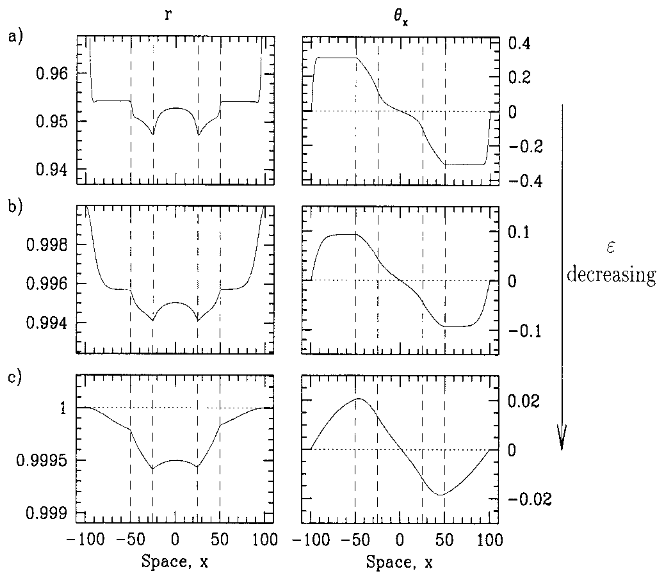

FIG. 6. *Graphs illustrating the change in the form of the steady solution on a large domain when* ε *is decreased, for* (a) $\varepsilon = 0.1$, (b) $\varepsilon = 0.01$, *and* (c) $\varepsilon = 0.001$ *(solid lines). The dashed lines indicate the region boundaries* $(-x_2, -x_1, x_1, x_2)$. *The solutions shown are for* (9) *with* $\rho_\lambda = -1$, $\rho_\omega = 0$ $(\omega_0(x) \equiv 1)$, $\Omega_0 = -1/2$, $\Omega_1 = 1$, *where* $f(x)$ *is given in* (10), *and is plotted at* $t = 2000$ *from an initial periodic plane-wave of stable amplitude* $\hat{r} = 0.9$.

the solution no longer settles down to a steady state. Instead, the point at which $\theta_x = 0$ oscillates between $-x_2$ and x_2, with a similar oscillation in the shape of r). Equivalently, periodic plane-waves will not appear on large domains if ε is taken sufficiently small (the critical size of which is dependent upon the domain size), as illustrated in Figure 6(c).

On large domains, the form of the periodic plane-waves which develop when λ_0 is decreased in the center is dependent upon the value of ε; smaller values of ε lead to waves with an amplitude closer to 1 (the limit cycle amplitude) and a frequency closer to 0, until they are no longer evident for very small ε. This is because the size of the region of the domain in which they form—where flat sections of the r, θ_x plots are seen—shrinks as ε decreases; it is "eaten into" by boundary effects. This is illustrated in the sequence of graphs in Figure 6. Decreasing the values of x_1 and x_2 also has the effect of increasing the amplitude and decreasing the frequency of the selected periodic plane-wave; only very slowly at first, but then faster, as $x_1,\ x_2 \to 0$. This effect is illustrated by the series of graphs in Figure 7. The value of x_2 can also affect the extent of the plane-waves: intuitively, a value of x_2 closer to $x_{\max}$ leaves less room for the plane-waves, as they only occur in regions outside of $-x_2 < x < x_2$.

The complete difference in the form of the solutions when λ_0 is increased or decreased in the center of a large domain is striking. When λ_0 is decreased, the symmetry of the domain is maintained by the solution which evolves from the nonsymmetric initial conditions—a one-dimensional target pattern. The same is true of the solution on a smaller domain (for a fixed ε) (compare Figures 5(a) and (b)). However, when λ_0 is increased, the domain symmetry is broken by the solution which evolves on a large domain, whereas it is maintained on small domains (compare Figures 5(c) and (d)). Symmetry breaking must then occur as the domain size is increased, with ε

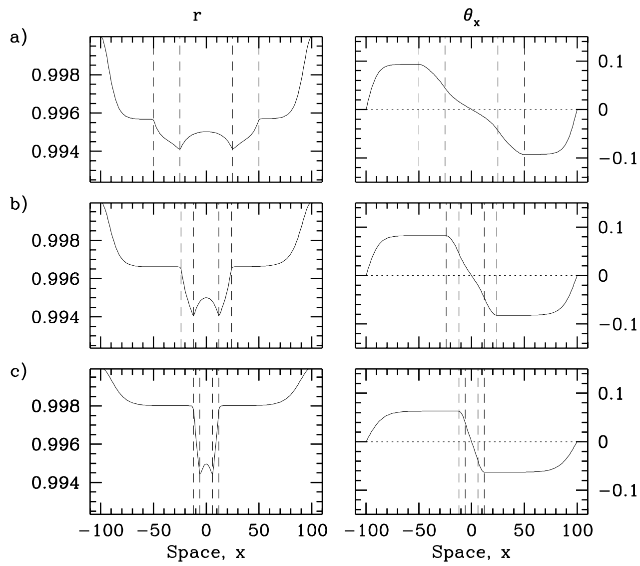

FIG. 7. *Graphs illustrating the change in the form of the steady solution on a large domain when x_1 and x_2 are decreased. The sequence shows that, as x_1 and x_2 decrease, the amplitude of the periodic plane-waves, r, moves closer to the limit cycle amplitude, 1, and the spatial frequency of the periodic plane waves, θ_x, decreases to 0. The dashed lines indicate the region boundaries $(-x_2, -x_1, x_1, x_2)$, which are taken as* (a) $x_1 = 25$, $x_2 = 50$; (b) $x_1 = 12$ $x_2 = 24$; *and* (c) $x_1 = 6$, $x_2 = 12$ *(solid lines). The solutions shown are for* (9) *with* $\rho_\lambda = -1$, $\rho_\omega = 0$ $(\omega_0(x) \equiv 1)$, $\Omega_0 = -1/2$, $\Omega_1 = 1$, *where $f(x)$ is given in* (10) *and* $\varepsilon = 0.01$, *plotted at* $t = 3000$ *from an initial periodic plane-wave of stable amplitude* $\hat{r} = 0.9$.

fixed (or, alternatively, as ε is increased on a fixed domain). We now investigate this behavior in more detail by constructing an analytical approximation to the solution, by treating (9) as a perturbation problem in the small parameter ε.

4. Perturbation solution for piecewise linear $\boldsymbol{\lambda_0}$. In this section, we study analytically the case of piecewise linear spatial variation of the parameter λ_0, as defined by the function $f(\cdot)$ in (10), with ω_0 constant ($\rho_\omega = 0$). To do this we solve for steady state solutions of the equations (9), by expanding for small ε, separately in the three regions $0 < x < x_1$, $x_1 < x < x_2$, and $x_2 < x < x_{\max}$. We then join these solutions, and apply boundary conditions at $x = 0$ and $x = x_{\max}$; we require that r is symmetrical about $x = 0$, with θ_x antisymmetric, so that $r_x(0) = \theta_x(0) = 0$.

4.1. Regular solution of the problem. We look for steady solutions of (6), satisfying $r_t = 0$ and $\theta_t = \sigma$, where σ is an unknown constant, independent of time. Note that the solution we are looking for is a steady state for r and θ_x, but not for θ: u and v continue to oscillate. If we then write $\phi = r'/r$ and $\psi = \theta'$ (where $'$ is d/dx), (9) becomes

(11a) $$r' = \phi r,$$

(11b) $$\phi' = \psi^2 - \phi^2 + r^2 - 1 - \rho_\lambda \varepsilon f(x),$$

(11c) $$\psi' = \sigma(\varepsilon) - 2\phi\psi + \Omega_1 r^2 - \Omega_0,$$

where we have used $\lambda_0(x) = 1 + \rho_\lambda \varepsilon f(x)$ with $\rho_\lambda = \pm 1$, where $f(x)$ is as in (10).

We then assume a series solution of (11), in each of the three regions, of the form

$$\begin{aligned}
r(x;\varepsilon) &= r_0(x) + \gamma_1(\varepsilon) r_1(x) + \dots\ ,\\
\phi(x;\varepsilon) &= \phi_0(x) + \alpha_1(\varepsilon)\phi_1(x) + \dots\ ,\\
\psi(x;\varepsilon) &= \psi_0(x) + \delta_1(\varepsilon)\psi_1(x) + \dots\ ,\\
\sigma(\varepsilon) &= \sigma_0 + \beta_1(\varepsilon)\sigma_1 + \dots\ ,
\end{aligned}$$

where $\gamma_1,\ \alpha_1,\ \delta_1$, and β_1 are functions of ε to be determined, but which tend to zero as $\varepsilon \to 0$. Substitution of these forms into (11) then gives leading-order solutions of $r_0(x) = 1$, $\phi_0(x) = \psi_0(x) = 0$ (and $\sigma_0 = \Omega_0 - \Omega_1$); this is as expected, since when $\varepsilon = 0$ there is no variation of parameters across the domain, and so the only steady solution on the finite domain with zero-flux boundary conditions is the limit cycle. The equations for the higher-order terms then depend on the region being considered.

In the center region, $0 < x < x_1$, $f(x) \equiv 1$, and so the next-order terms in (11) give the equations

$$\gamma_1 r_1' = \alpha_1 \phi_1, \tag{12a}$$

$$\alpha_1 \phi_1' = \delta_1^2 \psi_1^2 + 2\gamma_1 r_1 - \rho_\lambda \varepsilon, \tag{12b}$$

$$\delta_1 \psi_1' = \beta_1 \sigma_1 + 2\Omega_1 \gamma_1 r_1. \tag{12c}$$

For these equations there are two distinguished limits; that is, there are two possible expansions for which a maximum number of terms in (12) are of leading order. Usually, the appropriate rescaling in a perturbation theory problem is a distinguished limit in this sense. In this case, the two possibilities are $\gamma_1 = \alpha_1 = \delta_1^2 = \beta_1^2 = \varepsilon$, or $\gamma_1 = \alpha_1 = \delta_1 = \beta_1 = \varepsilon$. Detailed consideration of both cases shows that it is the second of these two limits which is important. In this case, we have to solve

$$r_1' = \phi_1, \tag{13a}$$

$$\phi_1' = 2r_1 - \rho_\lambda, \tag{13b}$$

$$\psi_1' = \sigma_1 + 2\Omega_1 r_1, \tag{13c}$$

which, using our requirements that r be even and ψ odd about $x = 0$, gives

$$r_1^{(c)} = \frac{A_c}{2}\left(e^{\sqrt{2}x} + e^{-\sqrt{2}x}\right) + \frac{\rho_\lambda}{2}, \tag{14a}$$

$$\phi_1^{(c)} = \frac{A_c}{\sqrt{2}}\left(e^{\sqrt{2}x} - e^{-\sqrt{2}x}\right), \tag{14b}$$

$$\psi_1^{(c)} = \frac{A_c}{\sqrt{2}}\Omega_1\left(e^{\sqrt{2}x} - e^{-\sqrt{2}x}\right) + \sigma_1 x + \rho_\lambda \Omega_1 x \tag{14c}$$

in the center region (c), $0 < x < x_1$, where A_c is the one remaining constant of integration. Similarly we can find solutions in each of the other two regions, with this same distinguished limit. Specifically, we obtain

$$r_1^{(m)} = \frac{1}{2}\left(A_m e^{\sqrt{2}x} + B_m e^{-\sqrt{2}x}\right) + C(x_2 - x), \tag{15a}$$

$$\phi_1^{(m)} = \frac{1}{\sqrt{2}}\left(A_m e^{\sqrt{2}x} - B_m e^{-\sqrt{2}x}\right) - C, \tag{15b}$$

$$\psi_1^{(m)} = \frac{1}{\sqrt{2}}\Omega_1\left(A_m e^{\sqrt{2}x} - B_m e^{-\sqrt{2}x}\right) - C\Omega_1 x^2 + (2C\Omega_1 x_2 + \sigma_1)x + c_m \tag{15c}$$

in the middle region (m), $x_1 < x < x_2$, and

$$r_1^{(o)} = \frac{1}{2}\left(A_o e^{\sqrt{2}x} + B_o e^{-\sqrt{2}x}\right), \tag{16a}$$

$$\phi_1^{(o)} = \frac{1}{\sqrt{2}}\left(A_o e^{\sqrt{2}x} - B_o e^{-\sqrt{2}x}\right), \tag{16b}$$

$$\psi_1^{(o)} = \frac{1}{\sqrt{2}}\Omega_1\left(A_o e^{\sqrt{2}x} - B_o e^{-\sqrt{2}x}\right) + \sigma_1 x + c_o \tag{16c}$$

in the outside region (o), $x_2 < x < x_{\max}$, where $C = \rho_\lambda/2(x_2 - x_1)$ and A_m, B_m, c_m and A_o, B_o, c_o are constants of integration.

We can now join the center and middle solutions at $x = x_1$, and the middle and outside solutions at $x = x_2$, to determine the values of the constants A_m, B_m, c_m and A_o, B_o, c_o in terms of A_c, ρ_λ, x_1 and x_2. This gives the solution

(17)

$$\begin{aligned}
r_1^{(c)} &= A_c \cosh\sqrt{2}x + \frac{\rho_\lambda}{2},\\
\psi_1^{(c)} &= \Omega_1\sqrt{2}A_c \sinh\sqrt{2}x + (\sigma_1 + \rho_\lambda\Omega_1)x,\\
r_1^{(m)} &= A_c \cosh\sqrt{2}x + \frac{C}{\sqrt{2}}\sinh\sqrt{2}(x - x_1) + C(x_2 - x),\\
\psi_1^{(m)} &= \Omega_1\sqrt{2}A_c \sinh\sqrt{2}x + C\Omega_1\cosh\sqrt{2}(x - x_1) - C\Omega_1(x^2 - 2x_2 x + 1 + x_1^2) + \sigma_1 x,\\
r_1^{(o)} &= A_c \cosh\sqrt{2}x + \frac{C}{\sqrt{2}}\left(\sinh\sqrt{2}(x - x_1) - \sinh\sqrt{2}(x - x_2)\right),\\
\psi_1^{(o)} &= \Omega_1\sqrt{2}A_c \sinh\sqrt{2}x + C\Omega_1\left(\cosh\sqrt{2}(x - x_1) - \cosh\sqrt{2}(x - x_2) + x_2^2 - x_1^2\right) + \sigma_1 x.
\end{aligned}$$

Here we have not written the explicit solutions for ϕ_1 in each of the regions, as we always have $\phi_1 = r_1'$.

If we now apply the zero-flux boundary conditions to the outside solutions at $x = x_{\max}$, that is, $r_1'(x_{\max}) = 0$ and $\psi_1(x_{\max}) = 0$, we find

$$\sigma_1 = -\rho_\lambda\Omega_1\frac{x_1 + x_2}{2x_{\max}}, \tag{18a}$$

$$A_c = -\rho_\lambda \frac{\cosh\sqrt{2}(x_{\max}-x_1) - \cosh\sqrt{2}(x_{\max}-x_2)}{2\sqrt{2}(x_2-x_1)\sinh\sqrt{2}x_{\max}}. \tag{18b}$$

We remark that it is at this point that the solution using the alternative distinguished limit "fails," as the application of the zero-flux boundary conditions leads to the conclusion that $\psi_1^{(o)} = 0$, where $\psi^{(o)}(x) = 0 + \varepsilon^{1/2}\psi_1^{(o)}(x)$, and so we would have to look at the next terms in the series solution, which would be precisely those we have obtained using the second distinguished limit.

The asymptotic solution up to order ε is then

$$r(x;\varepsilon) = 1 + \varepsilon r_1(x), \tag{19a}$$

$$\theta_x(x;\varepsilon) = \varepsilon\psi_1(x), \tag{19b}$$

$$\sigma(\varepsilon) = \overline{\omega_0} - 1 + \varepsilon\sigma_1, \tag{19c}$$

where r_1 and ψ_1 are given in (17) for each region $0 < x < x_1$, $x_1 < x < x_2$ and $x_2 < x < x_{\max}$, and A_c and σ_1 are given in (18). The solutions for $x < 0$ are then produced by appropriate reflections of the solutions on $0 < x < x_1$, $x_1 < x < x_2$ and $x_2 < x < x_{\max}$, respectively, using the fact that r is even and ψ is odd about $x = 0$. This asymptotic solution thus fits well with the results of numerical simulations on domains which are sufficiently small for a given value of ε, or alternatively, for large domains given a sufficiently small ε (Figure 8). However, it cannot recreate the periodic plane-waves, which are seen only if ε or $x_{\max}$ are sufficiently large—the solution is not uniformly valid for large x, as terms in the solution which should be $\mathcal{O}(\varepsilon)$ become $\mathcal{O}(1)$ for x sufficiently large. The solution is thus only valid for larger domains if we decrease ε sufficiently.

4.2. Singular solution to the problem. Motivated by the form of the regular solution, we look for a solution valid on larger domains and for larger values of ε, which will show the regions of periodic plane-waves (i.e., constant r and θ_x). The perturbation problem is singular in this case, and a separate rescaling is required for values of x comparable with $1/\sqrt{\varepsilon}$. A full perturbation analysis would involve the use of two small parameters, ε and $1/x_{\max}$, since we require $x_{\max} \to \infty$ sufficiently fast as $\varepsilon \to 0$ in order for the solution to retain its form; however we do not attempt this. Rather, we adopt the simpler approach of rescaling separately for x small and large, and matching the two rescaled solutions. Numerical simulations indicate that it is necessary for x_2 to be large in order for target patterns to form clearly, and so we take $X_2 = \varepsilon^{1/2}x_2$, where X_2 is fixed as $\varepsilon \to 0$ ($x_2 = \mathcal{O}(\varepsilon^{-1/2})$). Thus we rescale x in both the outside and middle regions. The point x_1 can be large or small, in comparison to $1/\sqrt{\varepsilon}$, but we consider only the simpler case of small x_1, so that no rescaling is required in the center region.

Rescaling in the outside region. We begin by rescaling for large x, based at the boundary point $x_{\max}$; that is, we set $X_o = \nu(\varepsilon)(x - x_{\max})$, where ν is an unknown function of ε to be determined by matching, but with $\nu(\varepsilon) \to 0$ as $\varepsilon \to 0$. We then let $r(x) = R(X_o)$, $\phi(x) = \Phi(X_o)$, and $\psi(x) = \Psi(X_o)$, and rewrite equation (11) in terms of X;

$$\nu\frac{dR}{dX_o} = \Phi R, \tag{20a}$$

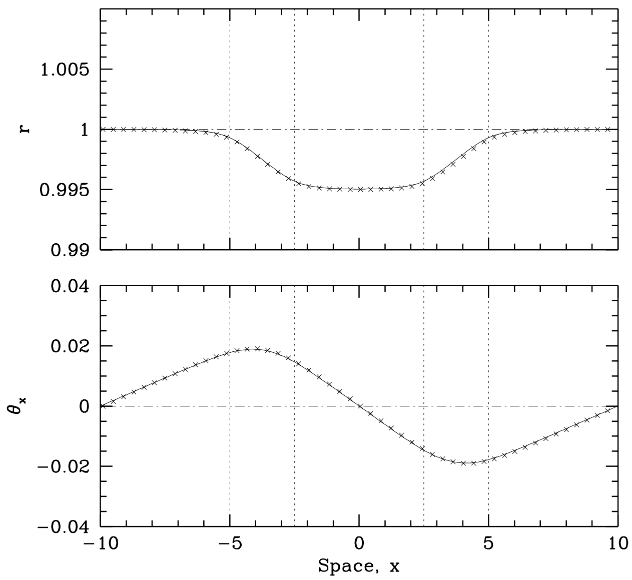

FIG. 8. *Graphs illustrating the match of our approximate solution* (19) *(solid lines) with numerical solutions (crosses) on small domains when λ_0 is decreased in the center of the domain ($\rho_\lambda = -1$). The comparison is excellent. The dotted lines indicate the region boundaries ($-x_2, -x_1, x_1, x_2$). The numerical solutions are for* (9) *with $\lambda_0(x) = 1 + \rho_\lambda \varepsilon f(x)$, $\Omega_0 = -1/2$ and $\Omega_1 = 1$, where $f(x)$ is given in* (10), *$x_{\max} = 10$, $x_2 = 5$, $x_1 = 2.5$ and $\varepsilon = 0.01$, plotted at $t = 2000$ from an initial periodic plane-wave of stable amplitude $\hat{r} = 0.9$. The comparison is just as good in the case when λ_0 is increased in the center of the domain ($\rho_\lambda = +1$), but the r solutions are reflected in $r = 1$ and the θ_x solutions are reflected in $\theta_x = 0$.*

(20b)
$$\nu \frac{d\Phi}{dX_o} = \Psi^2 - \Phi^2 + R^2 - 1,$$

(20c)
$$\nu \frac{d\Psi}{dX_o} = \sigma(\varepsilon) - 2\Phi\Psi + \Omega_1 R^2 - \Omega_0.$$

We assume a series solution of (20) of the form

$$\begin{aligned} R(X_o;\varepsilon) &= R_0(X_o) + \Gamma_1(\varepsilon) R_1(X_o) + \dots \ , \\ \Phi(X_o;\varepsilon) &= \Phi_0(X_o) + A_1(\varepsilon)\Phi_1(X_o) + \dots \ , \\ \Psi(X_o;\varepsilon) &= \Psi_0(X_o) + \Delta_1(\varepsilon)\Psi_1(X_o) + \dots \ , \\ \sigma(\varepsilon) &= \sigma_0 + \beta_1(\varepsilon)\sigma_1 + \dots \ , \end{aligned}$$

with $\Gamma_1, A_1, \Delta_1,$ and β_1 functions of ε which are $o(1)$ as $\varepsilon \to 0$. However, here $\sigma = \theta_t$ remains the same as for the regular solution, so that we have $\beta_1 = \varepsilon$. Again, when $\varepsilon = 0$ we know that the steady solution is the limit cycle, and so $R_0 \equiv 1$ and $\Phi_0 = \Psi_0 \equiv 0$. Substitution of these forms into (20) then gives the next-order equations

(21a)
$$\nu \Gamma_1 \frac{dR_1}{dX_o} = A_1 \Phi_1,$$

(21b)
$$\nu A_1 \frac{d\Phi_1}{dX_o} = \Delta_1^2 \Psi_1^2 + 2\Gamma_1 R_1,$$

$$\nu\Delta_1 \frac{d\Psi_1}{dX_o} = \varepsilon\sigma_1 + 2\Omega_1\Gamma_1 R_1. \tag{21c}$$

The distinguished limit of these equations is then $\nu = \Delta_1 = \Gamma_1^{1/2} = A_1^{1/3} = \varepsilon^{1/2}$. Thus we must solve the equation $d\Psi_1/dX_o + \Omega_1\Psi_1^2 = \sigma_1$, with $R_1 = -\Psi_1^2/2$ and $\Phi_1 = dR_1/dX_o$. There are four possible solutions of this:

$$\begin{aligned} \Psi_1 = \frac{a}{\Omega_1}\tan(-a(X_o+K)), \text{ or } \frac{a}{\Omega_1}\cot(a(X_o+K)) \quad \text{if } \ a^2 = -\sigma_1\Omega_1 > 0,\\ \text{or } \ \frac{a}{\Omega_1}\tanh(a(X_o+K)), \text{ or } \frac{a}{\Omega_1}\coth(a(X_o+K)) \quad \text{if } \ a^2 = \sigma_1\Omega_1 > 0, \end{aligned} \tag{22}$$

where K is the constant of integration in each case.

To get flat sections, corresponding to target patterns, we choose the tanh solution for Ψ_1, and by setting $K = 0$ we can then satisfy the zero-flux boundary conditions required at $x = x_{\max}$. Thus we have the solution in the outside region as

$$r^{(o)}(x) = R(\varepsilon^{1/2}(x - x_{\max})) = 1 - \varepsilon\frac{\sigma_1}{2\Omega_1}\tanh^2(\varepsilon^{1/2}\sqrt{\sigma_1\Omega_1}(x - x_{\max})), \tag{23a}$$

$$\psi^{(o)}(x) = \Psi(\varepsilon^{1/2}(x - x_{\max})) = \varepsilon^{1/2}\sqrt{\frac{\sigma_1}{\Omega_1}}\tanh(\varepsilon^{1/2}\sqrt{\sigma_1\Omega_1}(x - x_{\max})), \tag{23b}$$

to first order.

Note that in the case $\rho_\lambda = +1$, we see that we cannot construct a shock pattern using our above approximate solutions. This is because the shock requires $\psi > 0$ for $x > 0$, but

$$\psi^{(o)} = \varepsilon^{1/2}\sqrt{\frac{\sigma_1}{\Omega_1}}\tanh(\varepsilon^{1/2}\sqrt{\sigma_1\Omega_1}(x - x_{\max})) < 0 \quad \text{ for all } x \in (x_2, x_{\max}).$$

This provides some validation for our results from the numerical simulations with a piecewise linear parameter variation in section 3, where we observed that $\rho_\lambda = +1$ gave just one band of periodic plane-waves in the center region; not a shock pattern, as we might have expected given the target pattern in the case $\rho_\lambda = -1$. However, this is not absolute proof that such a shock solution does not exist: It remains a possibility that one of the other three possible solutions in (22) for Ψ_1 could give a solution in the form of a shock, but we have not investigated this.

Rescaling in the middle region. To find an approximate solution in the middle region, it is necessary for us to find a composite between a rescaled solution and an unrescaled solution in this region. We only do this for the case $\rho_\lambda = -1$ (λ_0 decreased in the center of the domain), as this is the case that gives the target pattern we are attempting to approximate; we have already demonstrated that it is not possible to get a shock pattern in the case $\rho_\lambda = +1$ as a mirror image of the target for $\rho_\lambda = -1$, as the outside region solution does not have the required form for this.

We must first recalculate our unrescaled solution, under the assumption $x_2 = \mathcal{O}(\varepsilon^{-1/2})$ rather than $\mathcal{O}(1)$, as was used in section 4.1. Writing $X_2 = \varepsilon^{1/2}x_2$ in (11) with $f(x) = (x_2 - x)/(x_2 - x_1) = (X_2 - \varepsilon^{1/2}x)/(X_2 - \varepsilon^{1/2}x_1) = 1$ to leading order, and again assuming solutions in the form $r(x) = 1 + \gamma_1(\varepsilon)r_1(x) + \dots$, $\phi(x) = \alpha_1(\varepsilon)\phi_1(x) + \dots$, $\psi(x) = \delta_1(\varepsilon)\psi_1(x) + \dots$, gives the same distinguished limit as previously; $\gamma_1 = \alpha_1 = \delta_1 = \varepsilon$. Solving the leading-order equations then gives

$$r^{(m)} = 1 + \frac{\varepsilon}{2}\left(A_m e^{\sqrt{2}x} + B_m e^{-\sqrt{2}x}\right) - \frac{\varepsilon}{2}, \tag{24a}$$

(24b) $$\psi^{(m)} = \varepsilon\frac{\Omega_1}{\sqrt{2}}\left(A_m e^{\sqrt{2}x} - B_m e^{-\sqrt{2}x}\right) + \varepsilon(\sigma_1 - \Omega_1)x + \varepsilon c_m,$$

where $r^{(m)} = 1 + \varepsilon r_1^{(m)}$, $\psi^{(m)} = \varepsilon\psi_1^{(m)}$ to $\mathcal{O}(\varepsilon)$ and A_m, B_m, c_m are constants to be determined by matching and joining.

We now consider solutions in this middle region for large x, using the rescaling $X_m = \nu(\varepsilon)x$. We let $r(x) = R(X_m)$, $\phi(x) = \Phi(X_m)$, and $\psi(x) = \Psi(X_m)$, and rewrite (11) in terms of X_m in the middle region (where $f(x) = (x_2 - x)/(x_2 - x_1)$):

(25a) $$\nu\frac{dR}{dX_m} = \Phi R,$$

(25b) $$\nu\frac{d\Phi}{dX_m} = \Psi^2 - \Phi^2 + R^2 - 1 + \varepsilon\left(\frac{X_2 - X_m}{X_2 - \nu x_1}\right),$$

(25c) $$\nu\frac{d\Psi}{dX_m} = \sigma(\varepsilon) - 2\Phi\Psi + \Omega_1 R^2 - \Omega_0.$$

We again assume a series solution of (25) of the form

$$\begin{aligned} R(X_m;\varepsilon) &= 1 + \Gamma_1(\varepsilon)R_1(X_m) + \dots\ , \\ \Phi(X_m;\varepsilon) &= A_1(\varepsilon)\Phi_1(X_m) + \dots\ , \\ \Psi(X_m;\varepsilon) &= \Delta_1(\varepsilon)\Psi_1(X_m) + \dots\ , \\ \sigma(\varepsilon) &= \Omega_0 - \Omega_1 + \varepsilon\sigma_1 + \dots\ , \end{aligned}$$

with Γ_1, A_1, Δ_1, and β_1 functions of ε which are $o(1)$ as $\varepsilon \to 0$. (We have again assumed the limit cycle solution when $\varepsilon = 0$.) Substitution of these forms into (25) then gives the next-order equations

(26a) $$\nu\Gamma_1\frac{dR_1}{dX_m} = A_1\Phi_1,$$

(26b) $$\nu A_1\frac{d\Phi_1}{dX_m} = \Delta_1^2\Psi_1^2 + 2\Gamma_1 R_1 + \varepsilon\frac{1}{X_2}(X_2 - X_m),$$

(26c) $$\nu\Delta_1\frac{d\Psi_1}{dX_m} = \varepsilon\sigma_1 + 2\Omega_1\Gamma_1 R_1.$$

The distinguished limit of these equations is then $\nu = \Delta_1 = \Gamma_1^{1/2} = A_1^{1/3} = \varepsilon^{1/2}$. Thus we must solve the equation

(27) $$\frac{d\Psi_1}{dX_m} + \Omega_1\Psi_1^2 = \frac{\Omega_1}{X_2}\left(X_m + \frac{X_2}{\Omega_1}(\sigma_1 - \Omega_1)\right),$$

with $R_1 = -\Psi_1^2/2 - (X_2 - X_m)/2X_2$ and $\Phi_1 = dR_1/dX_m$. The general solution of (27) can be written in terms of Airy functions, $Ai(\cdot), Bi(\cdot)$, as

(28) $$\Psi_1(X_m) = \frac{1}{(\Omega_1 X_2)^{1/3}}\left(\frac{Ai'(z) + Q\ Bi'(z)}{Ai(z) + Q\ Bi(z)}\right),$$

where $z = \dfrac{\Omega_1^{2/3}}{X_2^{1/3}}\left(X_m + \dfrac{X_2}{\Omega_1}(\sigma_1 - \Omega_1)\right)$, and Q is a constant of integration to be determined.

To match the unrescaled and rescaled solutions in the middle region we use the intermediate limit $x_\eta = \eta(\varepsilon)x$, with $\varepsilon^{1/2} \ll \eta(\varepsilon) \ll 1$. We first consider matching of the ψ solutions, where, in terms of the x_η, the unrescaled solution is

$$\psi^{(m)} \sim -\frac{\varepsilon}{\eta}(1-\sigma_1)x_\eta$$

to leading order if $A_m = 0$. (The unrescaled and rescaled solutions will never match if the unrescaled solution is allowed to increase exponentially with x, and so we must have $A_m = 0$.) The rescaled solution in the middle region, in terms of x_η, is

$$\Psi^{(m)}(X_m) = \varepsilon^{1/2}\Psi_1(X_m) = \varepsilon^{1/2}\Psi_1(\varepsilon^{1/2}x_\eta/\eta) = \frac{\varepsilon^{1/2}}{(\Omega_1 X_2)^{1/3}}\left(\frac{Ai'(z) + Q\ Bi'(z)}{Ai(z) + Q\ Bi(z)}\right),$$

where $z = \Omega_1^{2/3}\left(X_m + \frac{X_2}{\Omega_1}(\sigma_1 - \Omega_1)\right)/X_2^{1/3}$. By Taylor expanding the Airy functions about $z_0 = X_2^{2/3}(\sigma_1 - \Omega_1)/\Omega_1^{1/3}$, we can see that in order for this rescaled solution to match with the unrescaled solution to order ε/η, two conditions must be satisfied:

$$Ai'(z_0) + Q\ Bi'(z_0) = 0, \tag{29}$$

$$\frac{Ai''(z_0) + Q\ Bi''(z_0)}{Ai(z_0) + Q\ Bi(z_0)} = z_0. \tag{30}$$

The latter condition (30) is simply the differential equation for Airy functions, and so is automatically satisfied, thus we are left with (29), which will enable us to calculate σ_1 once we have determined Q. The r solutions match with no further conditions, and we have the composite solutions in the middle region

$$r^{(m)}_{\text{comp}}(x) = 1 - \frac{\varepsilon}{2} + \varepsilon\frac{B_m}{2}e^{-\sqrt{2}x} - \frac{\varepsilon}{2}\Psi_1^2(\varepsilon^{1/2}x) + \frac{\varepsilon^{3/2}}{2}\frac{x}{X_2}, \tag{31a}$$

$$\psi^{(m)}_{\text{comp}}(x) = \varepsilon^{1/2}\Psi_1(\varepsilon^{1/2}x) - \varepsilon\frac{B_m\Omega_1}{2}e^{-\sqrt{2}x} + \varepsilon c_m, \tag{31b}$$

where Ψ_1 is given by (28).

Joining solutions at the region boundaries. Now we must consider joining these composite middle region solutions with the central solutions at x_1 and the outside solutions at x_2, which are, respectively,

$$r^{(c)}(x) = 1 + \varepsilon\frac{A_c}{2}\left(e^{\sqrt{2}x} + e^{-\sqrt{2}x}\right) - \frac{\varepsilon}{2}, \tag{32a}$$

$$\psi^{(c)}(x) = \varepsilon\frac{A_c}{\sqrt{2}}\Omega_1\left(e^{\sqrt{2}x} - e^{-\sqrt{2}x}\right) - \varepsilon(\Omega_1 - \sigma_1)x \tag{32b}$$

(from (19) and (14)) and

$$r^{(o)}(x) = 1 - \varepsilon\frac{\sigma_1}{2\Omega_1}\tanh^2(\varepsilon^{1/2}\sqrt{\sigma_1\Omega_1}(x - x_{\max})), \tag{33a}$$

$$\psi^{(o)}(x) = \varepsilon^{1/2}\sqrt{\frac{\sigma_1}{\Omega_1}}\tanh(\varepsilon^{1/2}\sqrt{\sigma_1\Omega_1}(x - x_{\max})), \tag{33b}$$

from (23).

Considering first the join at x_1, we need to expand $\Psi_1(\varepsilon^{1/2}x_1)$ in the middle solutions, for which we require expansions of the Airy functions and their derivatives at $z = X_2^{2/3}(\sigma_1 - \Omega_1)/\Omega_1^{1/3} + \varepsilon^{1/2}x_1\Omega_1^{2/3}/X_2^{1/3}$. We do this by Taylor expanding the Airy functions about $z_0 = -X_2^{2/3}(\Omega_1 - \sigma_1)/\Omega_1^{1/3}$ again, and using (29) and (30) we get $\Psi_1(\varepsilon^{1/2}x_1) \approx -\varepsilon^{1/2}(\Omega_1 - \sigma_1)x_1$. Thus we have

$$\begin{aligned}\psi^{(m)}_{\mathrm{comp}}(x_1) &\approx -\varepsilon\frac{B_m}{2}e^{-\sqrt{2}x_1} + \varepsilon c_m - \varepsilon(\Omega_1 - \sigma_1)x_1\\ &= \psi^{(c)}(x_1) = \varepsilon\frac{A_c}{\sqrt{2}}\Omega_1\left(e^{\sqrt{2}x_1} - e^{-\sqrt{2}x_1}\right) - \varepsilon(\Omega_1 - \sigma_1)x_1.\end{aligned} \tag{34}$$

Similarly

$$\begin{aligned}r^{(m)}_{\mathrm{comp}}(x_1) &= 1 - \frac{\varepsilon}{2} + \varepsilon\frac{B_m}{2}e^{-\sqrt{2}x_1}\\ &= r^{(c)}(x_1) = 1 - \frac{\varepsilon}{2} + \varepsilon\frac{A_c}{2}\left(e^{\sqrt{2}x_1} + e^{-\sqrt{2}x_1}\right)\end{aligned} \tag{35}$$

and

$$\begin{aligned}\phi^{(m)}_{\mathrm{comp}}(x_1) &= \frac{dr^{(m)}_{\mathrm{comp}}}{dx}(x_1) = -\varepsilon\frac{B_m}{\sqrt{2}}e^{-\sqrt{2}x_1}\\ &= \phi^{(c)}(x_1) = \frac{dr^{(c)}}{dx}(x_1) = \varepsilon\frac{A_c}{\sqrt{2}}\left(e^{\sqrt{2}x_1} - e^{-\sqrt{2}x_1}\right)\end{aligned} \tag{36}$$

to leading order, and so we must have $A_c = B_m = c_m = 0$.

All that remains to do is to join the middle and outside solutions at $x_2 = X_2/\varepsilon^{1/2}$, which should determine the value of the remaining unknown Q, after which we can determine the value of σ_1 from (29), and so predict the amplitude and frequency of the periodic plane waves in the target pattern formed when the parameter λ_0 is decreased in the center of the one-dimensional domain. We will only consider joining the ψ solutions at x_2, as the r and ϕ solutions then follow automatically, with no further conditions required. Evaluating the composite middle solution, (31b), at $x_2 = X_2/\varepsilon^{1/2}$ and equating with the outside solution (33b) at x_2 we have

$$\begin{aligned}\psi^{(m)}_{\mathrm{comp}}(x_2) &= \varepsilon^{1/2}\Psi_1(X_2)\\ &= \frac{\varepsilon^{1/2}}{(\Omega_1 X_2)^{1/3}}\left(\frac{Ai'(z_2) + Q\ Bi'(z_2)}{Ai(z_2) + Q\ Bi(z_2)}\right)\\ &= \psi^{(o)}(x_2) = \varepsilon^{1/2}\sqrt{\frac{\sigma_1}{\Omega_1}}\tanh(\sqrt{\sigma_1\Omega_1}(X_2 - X_{\max})),\end{aligned}$$

where $z_2 = \sigma_1 X_2^{2/3}/\Omega_1^{1/3}$ and $X_{\max} = \varepsilon^{1/2}x_{\max}$. So, rearranging, we have

$$Q = -\frac{\Omega_1^{1/6}Ai'(z_2) - \sqrt{\sigma_1}X_2^{1/3}\tanh(\sqrt{\sigma_1\Omega_1}(X_2 - X_{\max}))Ai(z_2)}{\Omega_1^{1/6}Bi'(z_2) - \sqrt{\sigma_1}X_2^{1/3}\tanh(\sqrt{\sigma_1\Omega_1}(X_2 - X_{\max}))Bi(z_2)}. \tag{37}$$

The full solution is then

$$
\begin{aligned}
r^{(c)} &= 1 - \frac{\varepsilon}{2},\\
\psi^{(c)} &= -\varepsilon(\Omega_1 - \sigma_1)x,\\
r^{(m)} &= 1 - \frac{\varepsilon}{2} - \frac{\varepsilon}{2(\Omega_1 X_2)^{2/3}}\left(\frac{Ai'(z) + Q\ Bi'(z)}{Ai(z) + Q\ Bi(z)}\right)^2,\\
\psi^{(m)} &= \frac{\varepsilon^{1/2}}{(\Omega_1 X_2)^{1/3}}\left(\frac{Ai'(z) + Q\ Bi'(z)}{Ai(z) + Q\ Bi(z)}\right),\\
r^{(o)} &= 1 - \varepsilon\frac{\sigma_1}{2\Omega_1}\tanh^2(\varepsilon^{1/2}\sqrt{\sigma_1\Omega_1}(x - x_{\max})),\\
\psi^{(o)} &= \varepsilon^{1/2}\sqrt{\frac{\sigma_1}{\Omega_1}}\tanh(\varepsilon^{1/2}\sqrt{\sigma_1\Omega_1}(x - x_{\max})),
\end{aligned}
\tag{38}
$$

where $z = \Omega_1^{2/3}(\varepsilon^{1/2}x - \frac{X_2}{\Omega_1}(\Omega_1 - \sigma_1))/X_2^{1/3}$, $X_2 = \varepsilon^{1/2}x_2$, Q is given by (37) and σ_1 is determined by the condition (29), which is

$$Ai'(z_0) + Q\ Bi'(z_0) = 0$$

with $z_0 = X_2^{2/3}(\sigma_1 - \Omega_1)/\Omega_1^{1/3}$.

It should be noted that this solution is valid only when x_1 is small, as we would have to rescale in the central region if x_1 were allowed to be large. Figure 9 illustrates the very good fit of the analytical approximation to the numerical solution, provided x_1 is small: here (29) and (37) have been solved numerically to calculate σ_1, which has the value 0.384 for parameters used in Figure 9. We can thus predict that the target patterns formed when the parameter λ_0 is decreased in the center of a one-dimensional domain (in a manner given by (10), where $x_1 = \mathcal{O}(1)$ and $x_2 = \mathcal{O}(\varepsilon^{-1/2})$) will have amplitude $r = 1 - \varepsilon\sigma_1/2\Omega_1 + o(\varepsilon)$ and frequency $\theta_x = \varepsilon^{1/2}\sqrt{\frac{\sigma_1}{\Omega_1}} + o(\varepsilon^{1/2})$, where σ_1 is determined from (29) with (37). Note that this is consistent with $\theta_x = \sqrt{\lambda(r)}$, as we expect for plane waves in λ–ω systems. We also have $\theta_t = \Omega_0 - \Omega_1 + \varepsilon\sigma_1 + o(\varepsilon) = \omega(r)$, as expected. The restriction to $x_1 = \mathcal{O}(1)$ means that we do not require a rescaling for large x in the central region; but this calculation could of course be carried out, were we to allow $x_1 = \mathcal{O}(\varepsilon^{-1/2})$. The matching of rescaled and unrescaled solutions would then occur in the central region, joining with just the rescaled solutions in the middle and outside regions. This would lead to an equation determining σ_1, and so give the amplitude and frequency of the target pattern produced in this case.

Using the rescalings (8), we see that the target patterns formed in the general system (7) would have

$$
\begin{aligned}
\widetilde{r} &= \sqrt{\frac{\overline{\lambda_0}}{\lambda_1}}\left(1 - \varepsilon\frac{\sigma_1}{2}\frac{\lambda_1}{\omega_1} + o(\varepsilon)\right),\\
\widetilde{\psi} = \widetilde{\theta}_{\tilde{x}} &= \varepsilon^{1/2}\sqrt{\frac{\sigma_1\overline{\lambda_0}\lambda_1}{\omega_1}} + o(\varepsilon^{1/2}),\\
\widetilde{\theta}_{\tilde{t}} &= \overline{\lambda_0}\left(\frac{\overline{\omega_0}\lambda_1 - \overline{\lambda_0}\omega_1}{\overline{\lambda_0}\lambda_1} + \varepsilon\sigma_1 + o(\varepsilon)\right).
\end{aligned}
$$

Using (37) and (29) to calculate σ_1 shows that it and $\sigma_1\lambda_1/\omega_1$ are increasing functions of $\Omega_1 = \omega_1/\lambda_1$; thus it can be determined how the amplitude and frequency

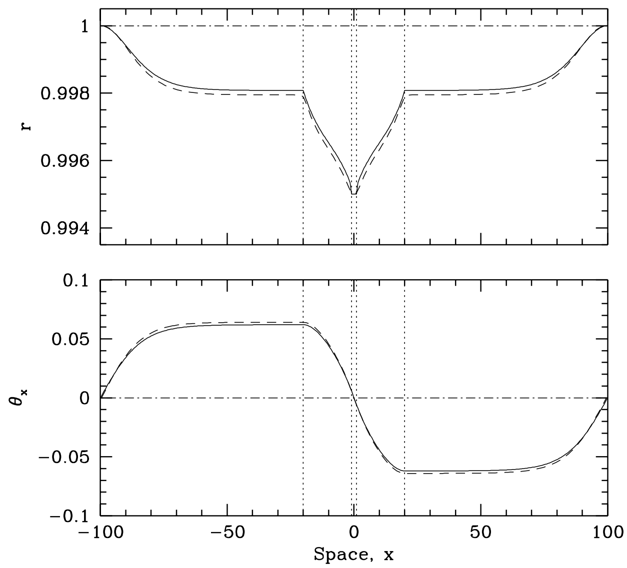

FIG. 9. *Graphs illustrating the comparison of our matched asymptotic solution* (38) *(solid lines) with a numerical solution (dashed lines), in the case where x_1 is sufficiently small ($\mathcal{O}(1)$) and x_2 is sufficiently large ($\mathcal{O}(1/\varepsilon^{1/2})$). The value of σ_1 is given by numerically solving* (29) *with* (37). *The dotted lines indicate the region boundaries ($-x_2, -x_1, x_1, x_2$). The plots are for $x_1 = 1$, $x_2 = 20$, $x_{\max} = 100$, and $\varepsilon = 0.01$, and the numerical solution is of* (5) *with $\lambda_0(x) = 1 - \varepsilon f(x)$ ($\rho_\lambda = -1$), where $f(x)$ is given by* (10), *and is plotted at $t = 2000$ from an initial periodic plane-wave of stable amplitude $\hat{r} = 0.9$.*

of the target patterns will change according to the values of each of the parameters $\overline{\omega_0}$, ω_1, $\overline{\lambda_0}$, λ_1, and ε. As these parameters can be related to the parameters in more general oscillatory reaction-diffusion equations close to Hopf bifurcation, it would be possible to predict how the target patterns produced there depend upon parameter values.

The case of piecewise linear parameter variation studied in this section is obviously quite different from the random variations used in section 2. Nevertheless, the analysis does give a clear insight into the way in which spatial variation of parameters is able to stabilize periodic wave patterns. The percentage variation must be sufficiently high in order that $1/\sqrt{\epsilon}$ is comparable with $x_{\max}$: in this case the addition of spatial variation is a singular perturbation problem in which periodic wave trains appear even though they are absent for uniform parameters. It is often clear, from plots like that shown in Figure 4, that in the case of random parameter variation, the targets have their centers (where $\theta_x = 0$) positioned on regions where λ_0 is below its average value. Of course, the random variation will produce many regions where λ_0 is decreased, and the detail of target center selection is a complex problem, outside the scope of our work.

5. Discussion. In this paper we have considered the long-term behavior after invasion of a finite region with spatial heterogeneity and zero-flux boundary conditions in oscillatory reaction-diffusion equations—in contrast to the homogeneous finite domains considered in [13]. In section 2 we used numerical simulations of several different predator-prey systems on spatially noisy domains. This showed that irregular wakes persist after the initial invasion. The effect on regular wakes depended critically on the amount of noise: a small percentage of noise in parameters had no affect on the die-out of the regular oscillations after invasion—it occured in the same manner as previously observed in [13] on homogeneous domains, so that the work presented there is still valid on finite domains with sufficiently small spatial variation of parameters. Large noise percentages, though, led to the persistence of regular oscillations across the domain—in a series of one or more target patterns. Increasing the noise still further led to the breakdown of the regular wakes to irregular-looking ones, which persist for a long time and throughout the domain. However, in most of these cases, and where target patterns are produced after invasion, continuing the numerical solution after halting the noisy spatial variation of parameters led to die-out of the spatial oscillations again, to the purely temporal oscillations of the limit cycle.

In section 3 we introduced λ–ω systems and verified that they mimic the behavior of regular oscillations on finite domains where the parameters are allowed to vary randomly with spatial position, as was observed for predator-prey systems. In particular, giving rise to target pattern solutions if there is a sufficiently large parameter variation. The same behavior is also observed for a piecewise linear spatial variation of the parameters on sufficiently large domains, with a target pattern appearing if the parameter is decreased in the center of the domain, but just one section of periodic plane-waves appearing if the parameter is increased there. On small domains however, periodic plane-waves are not apparent, but there is still a spatially inhomogeneous steady state attained. We then (section 4) obtain approximate solutions for the steady state attained for a λ–ω system with such a spatial variation of a parameter, both on large and small domains. This enabled us, in certain circumstances, to predict the the amplitude and frequency of the periodic plane-waves which will develop on large domains, given the variation of λ_0.

For ecology, the consequences of this work are two-fold. Ecologists are understandably sceptical about the results of theoretical work on a completely homogeneous domain, as real systems undoubtably contain some degree of spatial heterogeneity. Our results show that if this spatial heterogeneity manifests itself as noisy spatial variation of demographic parameters, and this noise is of a sufficiently small percentage, then the results gained by working on homogeneous domains still hold. However, larger environmental variations lead to the persistence of regular oscillations, via the production of target patterns. The detection of periodic plane-waves in ecological systems obviously requires a detailed analysis of spatiotemporal data. This has recently been carried out for vole populations in the Kielder forest [18], where statistical techniques were used to show that the observed spatially asynchronous, cyclically time-varying vole populations correspond to a periodic traveling wave.

It has long been known that impurities can facilitate the formation of target patterns in chemical systems (although such have certainly not been found at the center of every target pattern), and this work provides further numerical evidence for this. For the Belousov–Zhabotinskii reaction in the oscillatory regime, it has been demonstrated experimentally that temperature can affect the amplitude of the oscillation, with higher temperatures decreasing the amplitude [7, 8]. This could then provide a method of verifying our results on inhomogeneous finite domains experimentally: In a one-dimensional reaction vessel with temporal oscillations imposed at each end, such as that used by Stössel and Münster [34], stable periodic waves could be set up. Then the boundary conditions could be changed to zero-flux, and a different temperature imposed in a region around the center of the reaction vessel. Our work predicts that, for a sufficiently large temperature difference, the result should depend critically on whether the temperature in the center of the vessel is higher or lower than that for the rest of the vessel. If the central temperature is higher, then we expect a target pattern to form, whereas if the central temperature is lower, then we expect that the periodic plane-waves will die out; except for a band local to the region of lower temperature. Another possible experiment could involve oxygen or light, which are both known to affect the oscillations in the Belousov–Zhabotinskii reaction [35, 36, 26]. If the reactants were placed on a thin gel layer, in a reaction vessel that is closed except for a sheet over the top with randomly placed holes to allow oxygen or light to permeate through, then we could expect regular oscillations to be stabilized, in the form of target patterns, whereas they would otherwise have died out. Chemical experiments such as these provide the most effective method of testing our mathematical predictions.

Acknowledgment. We thank John Merkin for drawing our attention to the effects of oxygen on the Belousov–Zhabotinskii reaction.

REFERENCES

[1] D.L. Benson, P.K. Maini, and J.A. Sherratt, *Unravelling the Turing bifurcation using spatially varying diffusion coefficients*, J. Math. Biol., 37 (1998), pp. 381–417.
[2] P. Borckmans, *Competition in ramped Turing structures*, Phys. A, 188 (1992), pp. 137–157.
[3] R.S. Cantrell, C. Cosner, and V. Hutson, *Ecological models, permanence and spatial heterogeneity*, Rocky Mountain J. Math., 26 (1996), pp. 1–35.
[4] R.S. Cantrell and C. Cosner, *On the effects of spatial heterogeneity on the persistence of interacting species*, J. Math. Biol., 37 (1998), pp. 103–145.
[5] H.N. Comins, M.P. Hassell, and R.M. May, *The spatial dynamics of host-parasitoid systems*, J. Anim. Ecol., 61 (1992), pp. 735–748.
[6] S.R. Dunbar, *Traveling waves in diffusive predator-prey equations: Periodic orbits and point-to-periodic heteroclinic orbits*, SIAM J. Appl. Math., 46 (1986), pp. 1057–1077.
[7] A.K. Dutt and M. Menzinger, *Effect of stirring and temperature on the Belousov-Zhabotiskii reaction in a batch reactor*, J. Phys. Chem., 96 (1992), pp. 8447–8449.
[8] A.K. Dutt and S.C. Muller, *Effect of stirring and temperature on the Belousov-Zhabotiskii reaction in a CSTR*, J. Phys. Chem., 97 (1993), pp. 10059–10063.
[9] G.B. Ermentrout, X. Chen, and Z. Chen, *Transition fronts and localised structures in bistable reaction-diffusion systems*, Phys. D, 108 (1997), pp. 147–167.
[10] R.A. Fisher, *The wave of advance of advantageous genes*, Ann. Eugen., 7 (1937), pp. 353–369.
[11] P.S. Hagan, *Target patterns in reaction-diffusion systems*, Adv. Appl. Math., 2 (1981), pp. 400–416.
[12] R.D. Holt and M.P. Hassell, *Environmental heterogeneity and the stability of host-parasitoid interactions*, J. Anim. Ecol., 62 (1993), pp. 89–100.
[13] A.L. Kay and J.A. Sherratt, *On the persistence of spatiotemporal oscillations generated by invasion*, IMA J. Appl. Math., 63 (1999), pp. 199–216.
[14] N. Kopell and L.N. Howard, *Plane wave solutions to reaction-diffusion equations*, Stud. Appl. Math., 52 (1973), pp. 291–328.
[15] N. Kopell, *Target pattern solutions to reaction-diffusion equations in the presence of impurities*, Adv. Appl. Math., 2 (1981), pp. 389–399.
[16] N. Kopell and G.B. Ermentrout, *Phase Transitions and other phenomena in chains of coupled oscillators*, SIAM J. Appl. Math., 50 (1990), pp. 1014–1052.
[17] M. Kot, *Discrete-time traveling waves—ecological examples*, J. Math. Biol., 30 (1992), pp. 413–436.
[18] X. Lambin, D.A. Elston, S.J. Petty, and J.L. Mackinnon, *Spatial asynchrony and periodic travelling waves in cyclic populations of field voles*, Proc. Roy. Soc. London Ser. B, 265 (1998), pp. 1491–1496.
[19] K. Maginu, *Stability of periodic travelling wave solutions with large spatial periods in reaction-diffusion equations*, J. Differential Equations, 39 (1981), pp. 73–99.
[20] J.H. Merkin and M.A. Sadiq, *The dynamics of physiologically structured populations*, IMA J. Appl. Math., 57 (1996), pp. 273–309.
[21] J.D. Murray, *Mathematical Biology*, Springer-Verlag, Berlin, 1989.

[22] H.G. Othmer, *Current problems in pattern formation*, Lectures Math. Life Sci., 9 (1977), pp. 57–86.
[23] S.W. Pacala and J. Roughgarden, *Spatial heterogeneity and interspecific competition*, Theor. Pop. Biol., 21 (1982), pp. 92–113.
[24] M. Pascual, *Diffusion induced chaos in a spatial predator-prey system*, Proc. Roy. Soc. London Ser. B, 251 (1993), pp. 1–7.
[25] S.V. Petrovskii and H. Malchow, *A minimal model of pattern formation in a predator-prey system*, Math. Comput. Model., 29 (1999), pp. 49–63.
[26] M.K.R. Reddy, Z. Szlavik, Z. Nagyungvarai, and S.C. Muller, *Influence of light on the inorganic part of the ruthenium-catalysed Belousov-Zhabotinskii reaction*, J. Phys. Chem., 99 (1995), pp. 15081–15085.
[27] P. Rohani, T.J. Lewis, D. Grunbaum, and G.D. Ruxton, *Spatial self-organization in ecology: Pretty patterns or robust reality?*, Trends in Ecology and Evolution, 12, (1997), pp. 70–74.
[28] J.A. Sherratt, *Irregular wakes in reaction-diffusion waves*, Phys. D, 70 (1994), pp. 370–382.
[29] J.A. Sherratt, B.T. Eagan, and M.A. Lewis, *Oscillations and chaos behind predator-prey invasion: Mathematical artifact or ecological reality?*, Phil. Trans. Roy. Soc. London Ser. B, 352 (1997), pp. 21–38.
[30] J.A. Sherratt, *Invading wave fronts and their oscillatory wakes are linked by a modulated travelling phase resetting wave*, Phys. D, 117 (1998), pp. 145–166.
[31] N. Shigesada, *Traveling periodic waves in heterogeneous environments*, Theor. Pop. Biol., 30 (1986), pp. 143–160.
[32] J.C. Skellam, *Random dispersal in theoretical populations*, Biometrika, 38 (1951), pp. 196–218.
[33] J. Sneyd and J.A. Sherratt, *On the propagation of calcium waves in an inhomogeneous medium*, SIAM J. Appl. Math., 57 (1997), pp. 73–94.
[34] R. Stössel and A. F. Münster, *Periodic and irregular wave patterns in an open tubular gel reactor*, Chem. Phys. Lett., 239 (1995), pp. 354–360.
[35] L. Treindl, P. Ruoff, and P.O. Kvernberg, *Influence of oxygen and organic substrate on oscillations and autocatalysis in the Belousov-Zhabotinskii reaction*, J. Phys. Chem. A, 101 (1997), pp. 4606–4612.
[36] J.C. Wang, F. Hynne, P.G. Sorensen, and K. Nielson, *Oxygen influence on complex oscillations in a closed Belousov-Zhabotinsky reaction*, J. Phys. Chem., 100 (1996), pp. 17593–17598.
[37] P. Wiener and S. Tuljapurkar, *Migration in variable environments: Exploring life-history evolution using structured population models*, J. Theor. Biol., 166 (1994), pp. 75–90.
[38] A.T. Winfree, *Rotating chemical reactions*, Sci. Am., 230 (1974), pp. 82–95.
[39] J.X. Xin, *Existence and nonexistence of traveling waves and reaction-diffusion front propagation in periodic media*, J. Statist. Phys., 73 (1993), pp. 893–926.